Chapter 3

Parametric Study on Stabilized Red Mud

3.1 Introduction

In this chapter, two different methods namely conventional and experimental designed (*DOE*) are employed to study the affecting the strength and durability of stabilized red mud. Four different factors namely dry density, molding moisture content, amount of cementing materials and curing time has be taken based on the study reported in literature. Additionally, comparative studies based on conventional and experimental designed approach are also demonstrated and examined their performance in details and a part of the work has been published as (Kumar and Prasad, 2017) [2].

[2] **S. Kumar and A. Prasad**, "Parameters controlling strength of red mud-lime mix," *European Journal of Environmental and Civil Engineering*, pp. 1-15, 2017.

3.2 Selection of Molding Points

The various range of dry densities and molding moisture contents was selected based on compaction curve based on standard and modified effort. The dry unit weight and moisture content curves for the red mud with varying percentages of lime and different effort are shown in Fig.3.1. From Fig.3.1, it is observed that the maximum dry unit weight for the red mud decreased with the addition of lime. Further, it is also observed that the optimum moisture content of the red mud increased with the addition of lime. This increase in the optimum moisture content is due to the additional water was held within the flocs resulting from the flocculation due to the lime reaction. Further, the details of molding points adopted in preparing the red mud samples are shown in Fig.3.1.

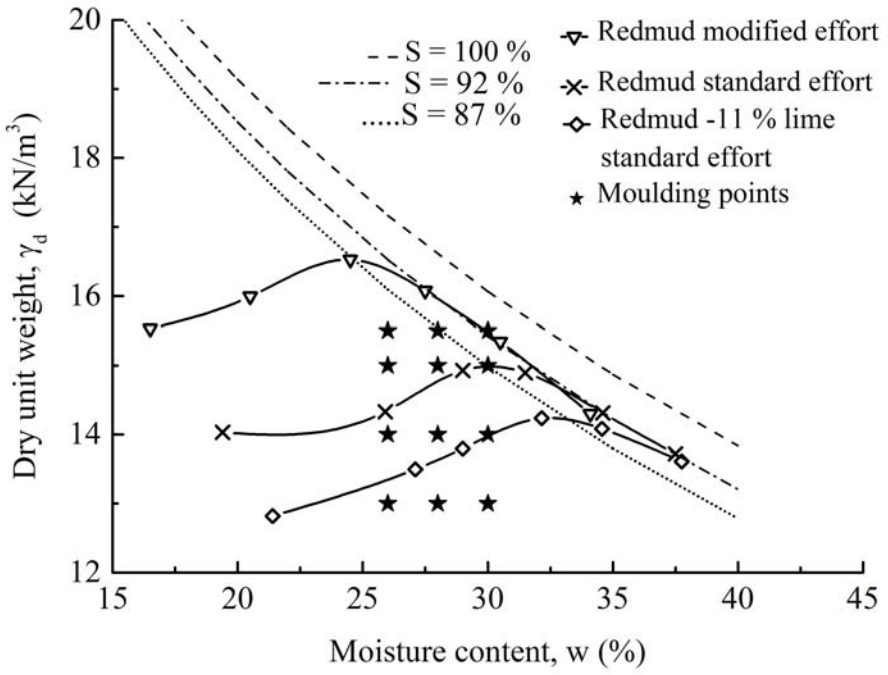

FIGURE 3.1: Compaction curves of red mud, red mud-lime and molding points

The molding points are located vertically and horizontally; vertical points represent constant moisture content and varying dry unit weights, whereas horizontal points represent constant dry unit weight and varying moisture contents. Table 3.1 summarizes the different parameters, their range used in the study.

TABLE 3.1: Summaries of various parameters and their ranges

Parameters	Range used	Remarks
Lime content (L) (%)	3, 5, 7, 9, and 11	Based on previous reported work
Curing Period (days)	7, 28 and 60	Based on previous reported work
Molding moisture content, (w) (%)	26, 28 and 30	From Compaction test (Present study)
Dry unit weight, γ_d (kN/m^3)	13, 14, 15, and 15.5	From Compaction test (Present study)
Wetting drying cycles , N	2, 7 and 12	Based on previous reported work

3.3 Planning of Experiment

In the first stage, the effect on red mud compressive strength by conventional design techniques is studied by various factors, such as mold humidity, dry density, cementing material dose and curing time.

In this chapter, the entire study has been planned in two phase. In first phase, the effect of various factors such as molding moisture, dry density, dose of cementing material and curing time on compressive strength of red mud has been studied using conventional design approach. Next, an alternative approach based on experimental design also known as an experimental designed approach is also tried to study the compressive strength of red mud. Finally, the performance of both the approaches are compared for further study.

Results and Discussion

3.4 Compressive Strength of Stabilized Red mud: Conventional Approach

3.4.1 Influence of Lime Content, Dry Density, Molding Moisture and Curing Time

In this section, a series of unconfined compressive strength tests have been carried out on the red mud. The variation of unconfined compressive strength of red mud with various factors such as dry density, lime content and curing are shown in Fig.3.2. It also shows the scatter plots and the possible best-fitted lines for distinct days cured red mud-lime mixture with distinct dry density and lime content. Further, an increase in the unconfined compressive strength of red mud with the increases in lime content and dry density is clearly seen from the Fig.3.2. A similar trend is also noticed for other curing periods. Figure.3.3 compares the variation of the strength of mix with curing time (3.3(a)) and molding moisture (3.3(b))and an increasing trends with curing time and a mild improvement in strength (q_u) is seen from the plots.

This increase in strength of red mud with the addition of lime as well as with the increase in the curing time is possibly due to any one or all the following factors.

- Flocculation of red mud particles by lime leading to the formation of large-sized aggregates.

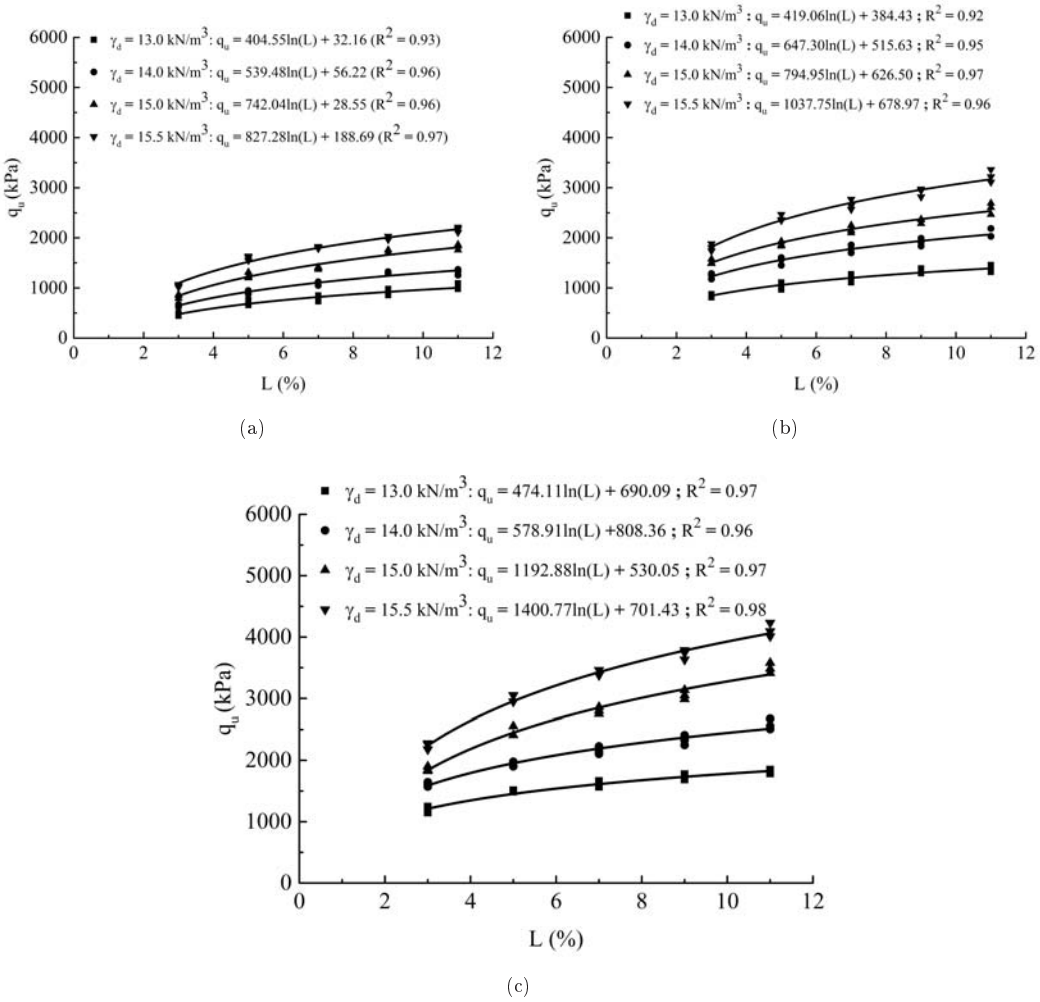

FIGURE 3.2: Influence of lime content and dry unit weight on q_u of red mud at varying curing time (a) 7 days, (b) 28 days, and (c) 60 days

- Cementing action due to carbonation of lime in the presence of atmospheric CO_2.

- Time dependent pozzolanic reactions occurring between free Calcium ions from lime and silica, and aluminum ions presents in red mud, forming cementitious in the presence of sufficient moisture (discussed in detail in sub sec. 1.3.1.1).

Whereas, the improvement in the unconfined compressive strength with

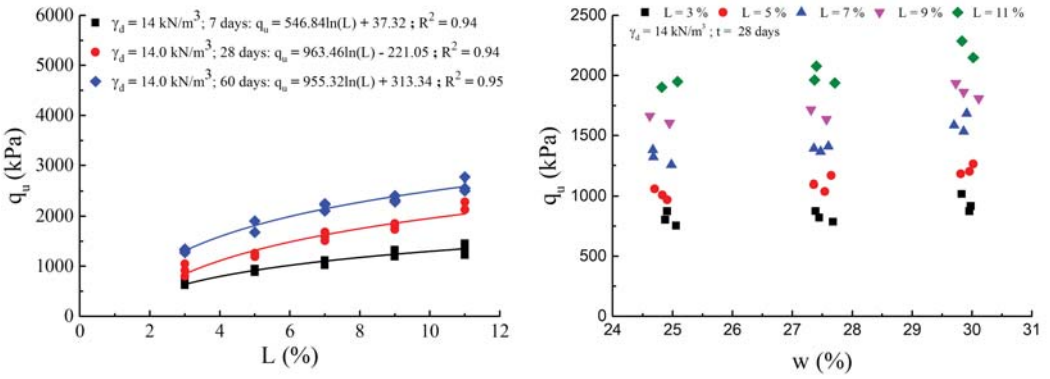

(a) (b)

FIGURE 3.3: Variation of (q_u) of red mud –lime mix with (a) curing time and (b) molding moisture content

the increase in the dry density is due to increase in the number of contact points among the particles in the red mud-lime matrix. The above reasons are in agreement with the findings discussed in Sec 3.4.2 and also reported by the other researchers [231, 232]. The improvement in the strength of red mud-lime mix is perhaps due to the formation of a different structure at the time of molding due to the addition of water. Similar observation was also made by [233] on the soil - lime mix. Further, it also confirms that the all factors have different influence over the behavior of strength of stabilized red mud.

3.4.2 Micro structural study

To investigate the morphological transformations of compacted red mud-lime mix, a series of scanning electron microscopy (SEM) and energy-dispersive X-ray spectroscopy (EDX) test has been performed on the failed sample of the unconfined compressive strength (q_u) test. Figure 3.4 present the SEM images (magnification = $10kX$) of red mud (Fig.3.4(a)), lime (Fig.3.4(b)) and cemented red mud-lime mix

(Figs.3.4(c-f)). In Figs.3.4(c-f), a relatively closed and denser structure (availability of a higher number of contacts) along with cementitious gel type formation in cemented red mud can be seen as compared to a relatively more porous matrix in case of raw red mud.

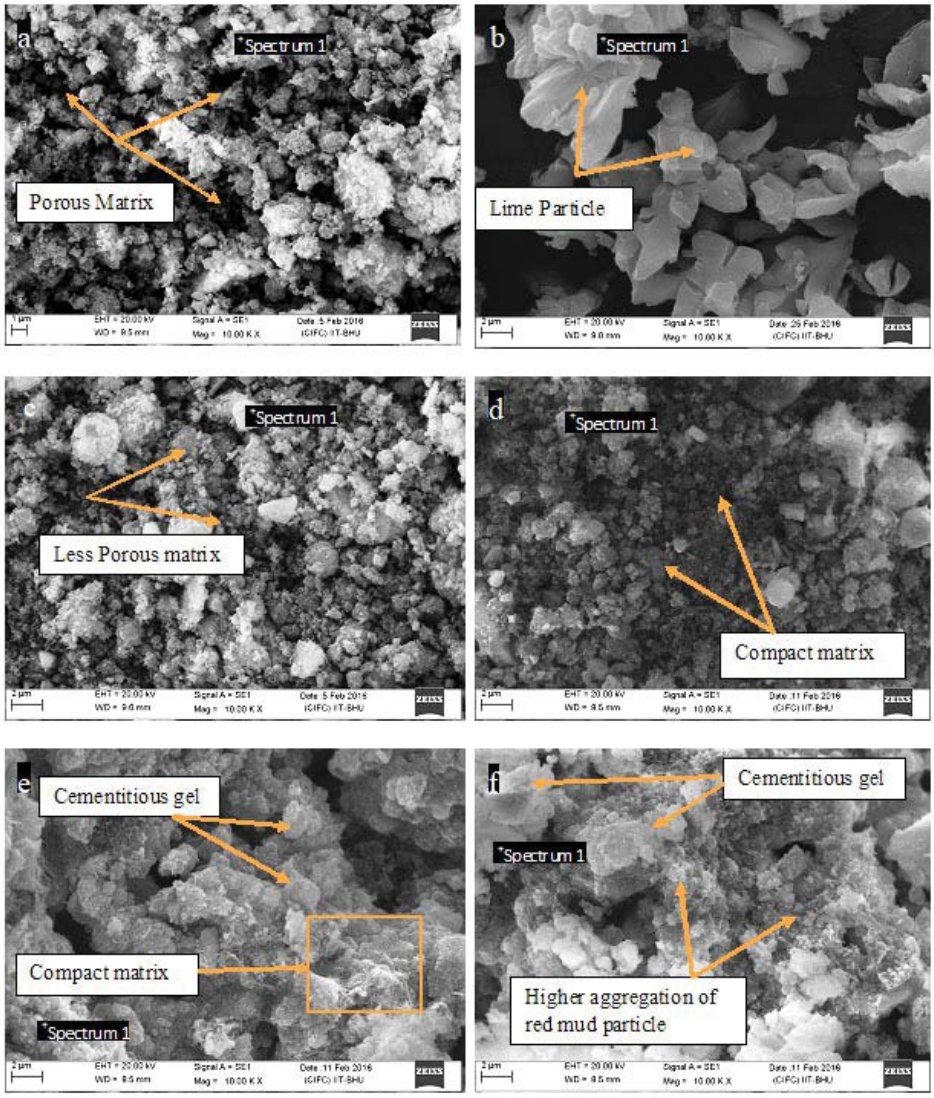

FIGURE 3.4: SEM images ($10kX$) of (a) red mud, (b) lime, (c) red mud + 3 % lime at density = 14 kN/m^3, (d) red mud + 3 % lime at density = 15.5 kN/m^3 (e) red mud + 9 % lime at density =14 kN/m^3, and (f) red mud + 9 % lime at density =15.5 kN/m^3

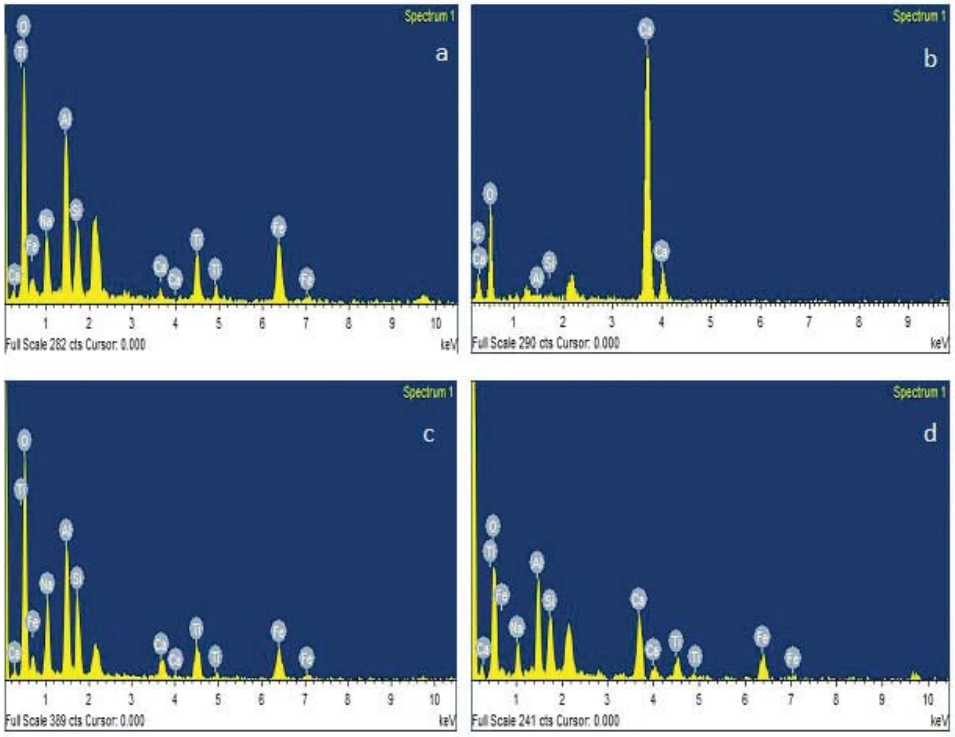

FIGURE 3.5: EDX of (a) red mud, (b) lime, (c) red mud + 3 % lime at density = 14 kN/m^3, and (d) red mud + 9 % lime at density = 14 kN/m^3

Figure 3.5 illustrates the energy-dispersive X-ray spectroscopy (EDX) of red mud (Fig. 3.5(a)), lime (Fig.3.5(b)) and cemented red mud-lime mix (Figs. 3.5(c-d)). From Fig. 3.5(a), it can be observed that red mud contains mainly Ca (1.35 %), Si (6.57 %), Al (10.86 %), Ti (12.55 %), and O (36.12 %) whereas, Ca (30.94 %) is a major component in case of lime (Fig. 3.5(b)). From Figs. 3.5(c-d) it appears that due to the addition of lime, peaks of Ca increases but that of Si and Al decreases which confirms that reactive Si and Al react with available Ca and formed cementitious gel by the pozzolanic reactions.

Thus, ratio of Ca/Si and Si/Al of red mud-lime mix is also studied and reported in Fig 3.6. It appears that Ca/Si ratio increases whereas Si/Al ratio decreases with the increase in lime content. Hence, the emissions of Ca, Si, Al, and

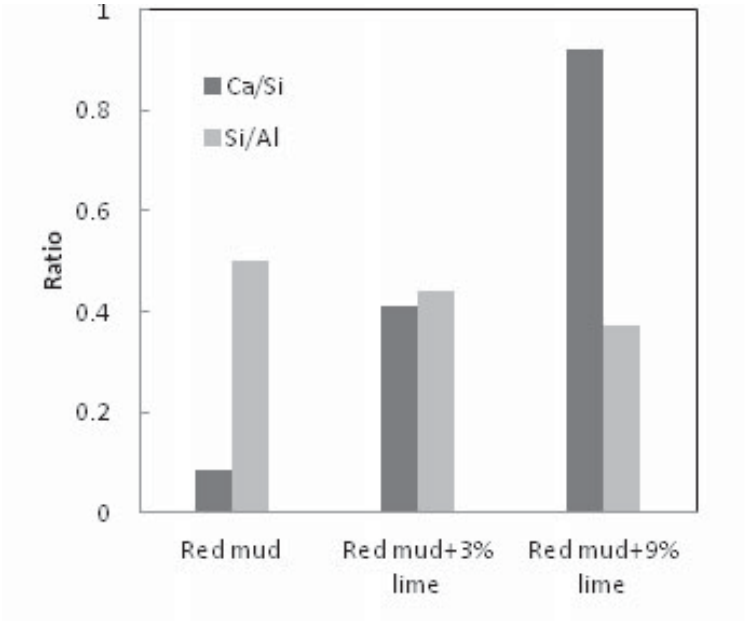

FIGURE 3.6: Variation of Ca/Si, and Si/Al ratio of red mud with binders

O spectrum confirm the formation of a cementing compound by pozzolanic reactions 1.1-1.2 leading to an increase in the unconfined compressive strength of the red mud with the addition of lime.

3.4.3 Predictive Equations

From the above section, it is clearly shown that a correlation of the compressive strength of stabilized red mud can be found with all factors. So various correlations for the same have been tried. First of all, general correlation using non-linear regression is created, then non-dimensional parameters such as the molding moisture/lime ratio (w/L) and the porosity/volume content of lime (η/L_v) are also introduced and discussed step by step in detail in the next sub-sections.

3.4.3.1 Linear Regression

Multiple regression is a statistical process which is use to obtain the best fit equation between several input and output. The general form of multiple linear regression equation may be expressed as:

$$Y = a + b_1 + X_1 + b_2X_2 + b_3X_3 + b_4X_4 \ldots\ldots b_nX_n \tag{3.1}$$

Where 'Y' is output, a is intercept of output, 'X_1' to 'X_1' are the input and 'b_1' to 'b_n' are the coefficients of inputs used to predict the output. In this trial, a linear analysis is carried out on the basis of experimental data sets (see Table. A.1, Appendix A), which predict compressive strength (qu) with a lime content (L), moisture content (w), dry density (γd), and curing time (t). The linear regression model equations obtained from experimental data sets for predicting the UCS are presented in the Eqn.3.2.

$$\boxed{q_u = -8595 + 41.8w + 22.06t + 527.5\gamma_d + 135.01L} \tag{3.2}$$

In addition, a more general correlation is also tested in the next section for a better understanding of stabilized red mud.

3.4.3.2 Molding moisture/lime ratio (w/L)

The variation of unconfined compressive strength of red mud with molding moisture / lime ratio (w/L) are shown in Fig. 3.7. Figure 3.7 offers q_u vs w/L plot for 28 days cured red mud-lime mix with distinct dry densities. A decreasing trend is observed from the plot and by observing the same, a power model is fitted well with fair correlations ($R^2 = 0.75$) for given dry densities.

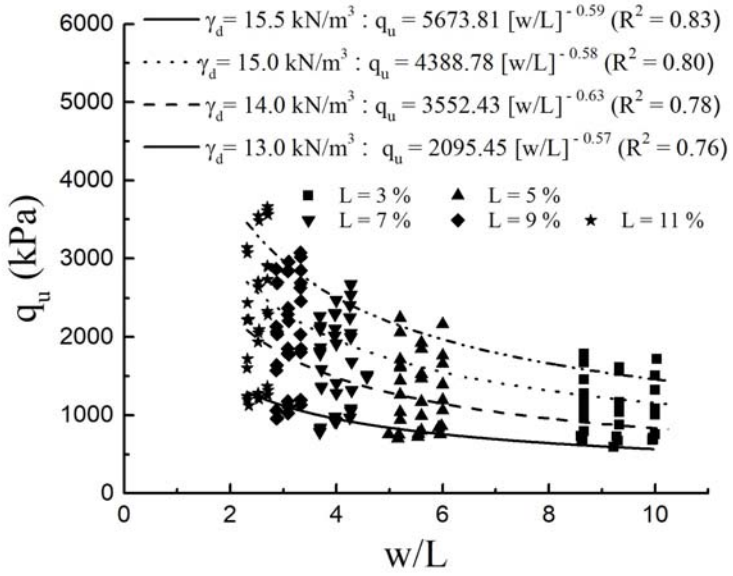

FIGURE 3.7: Variation of unconfined compressive strength (q_u) with water/lime ratio (w/L).

Further, to compare the trend in the variation of q_u vs w/L with different dry densities (γ_d), the exponent of the trend line required to be adjusted. In this study, the exponents is adjusted to an average exponent (0.60) of the individual trend line and same approach has been adopted for other curing periods.The details are shown in Fig. 3.8 and Eqs.(3.3-3.14).

For 7 days:

$$\gamma_d = 13.0\,kN/m^3;\ q_u = \ 1\ 799.65\ [^w/_L]^{-0.60} \tag{3.3}$$

$$\gamma_d = 14.0\,kN/m^3;\ q_u = \ 2\ 307.58\ [^w/_L]^{-0.60} \tag{3.4}$$

$$\gamma_d = 15.0\,kN/m^3;\ q_u = \ 3\ 235.56\ [^w/_L]^{-0.60} \tag{3.5}$$

$$\gamma_d = 15.5\,kN/m^3;\ q_u = \ 3\ 905.81\ [^w/_L]^{-0.60} \tag{3.6}$$

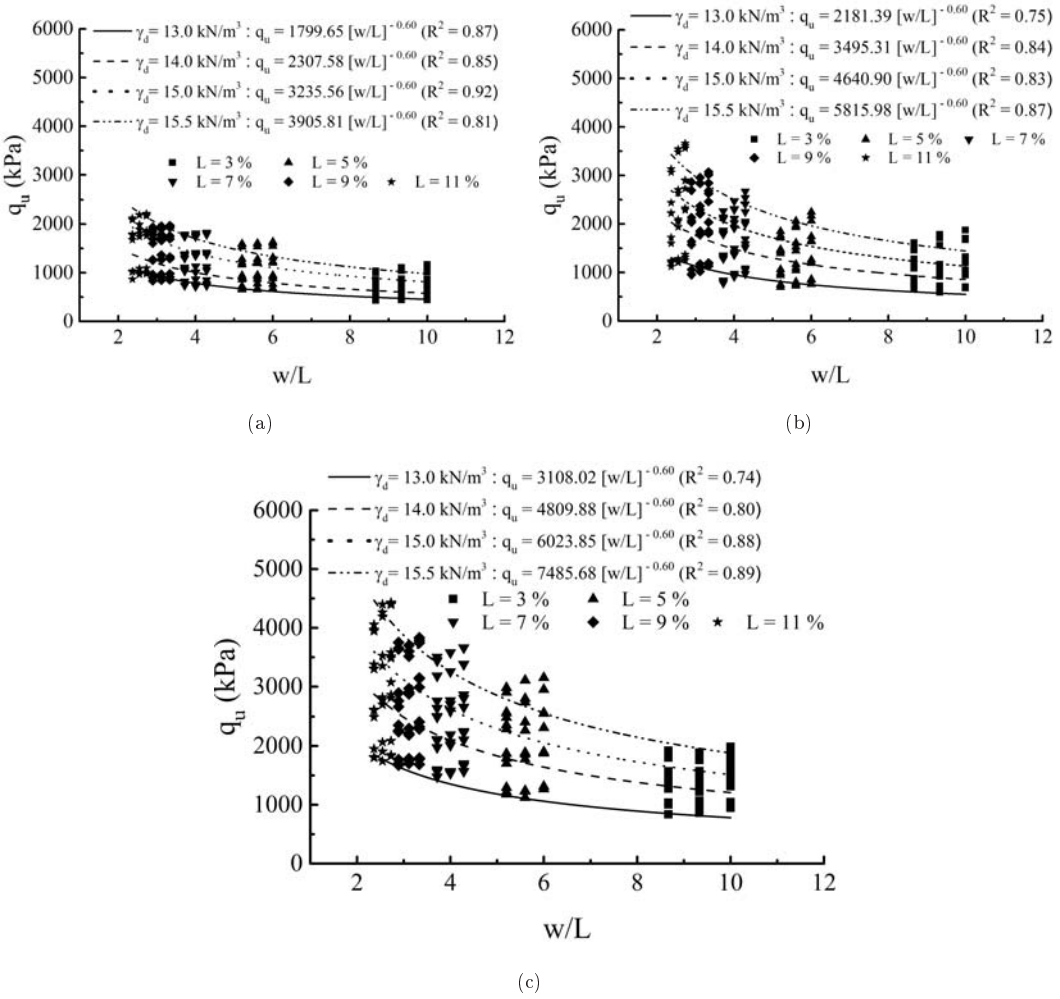

FIGURE 3.8: Variation of unconfined compressive strength (q_u) with adjusted water/lime ratio (w/L) (a) 7 days, (b) 28 days, and (c) 60 days

For 28 days:

$$\gamma_d = 13.0\,kN/m^3;\ q_u = \ 2\ 181.39\ [^w/_L]^{-0.60} \tag{3.7}$$

$$\gamma_d = 14.0\,kN/m^3;\ q_u = \ 3\ 495.31\ [^w/_L]^{-0.60} \tag{3.8}$$

$$\gamma_d = 15.0\,kN/m^3;\ q_u = \ 4\ 640.90\ [^w/_L]^{-0.60} \tag{3.9}$$

$$\gamma_d = 15.5\,kN/m^3;\ q_u = \ 5\ 815.98\ [^w/_L]^{-0.60} \tag{3.10}$$

For 60 days:

$$\gamma_d = 13.0\,kN/m^3;\ q_u = \ 3\ 108.02\ [^w/_L]^{-0.60} \tag{3.11}$$

$$\gamma_d = 14.0\,kN/m^3;\ q_u = \ 4\ 809.88\ [^w/_L]^{-0.60} \tag{3.12}$$

$$\gamma_d = 15.0\,kN/m^3;\ q_u = \ 6\ 023.85\ [^w/_L]^{-0.60} \tag{3.13}$$

$$\gamma_d = 15.5\,kN/m^3;\ q_u = \ 7\ 485.65\ [^w/_L]^{-0.60} \tag{3.14}$$

From Eqs.(3.3-3.14), it can be observed that q_u has a direct kinship with (w/L) and it differs by a scalar for different γ_d and curing time (t). For example, for 28 days cured specimen and dry density $(\gamma_d) = 13.0\ kN/m^3$, the ratio of $[q_u/(w/L)^{0.60}]$ is 2181.39 kPa which increases to 3495.31, 4640.90 and 5815.98 kPa with the increase in dry density (γ_d) to 14, 15 and 15.5 kN/m^3. Using same procedure, a distinctive relationship can also be established among q_u, w, L and γ_d and the results are presented in Fig.3.9) and in Eq.(3.15-3.17).

$$t = 7\,days;\ q_u = \ 0.008\ [^w/_L]^{-0.60}\ [\gamma_d]^{4.77} \tag{3.15}$$

$$t = 28\,days;\ q_u = \ 0.012\ [^w/_L]^{-0.60}\ [\gamma_d]^{4.77} \tag{3.16}$$

$$t = 60\,days;\ q_u = \ 0.015\ [^w/_L]^{-0.60}\ [\gamma_d]^{4.77} \tag{3.17}$$

Similarly, final relationship among q_u, w, L, γ_d and t is developed and are shown in Fig. 3.10 and presented in Eq. (3.18).

$$\boxed{q_u = \ 0.004\ [^w/_L]^{-0.60}\ [\gamma_d]^{4.77}\ [t]^{0.31}} \tag{3.18}$$

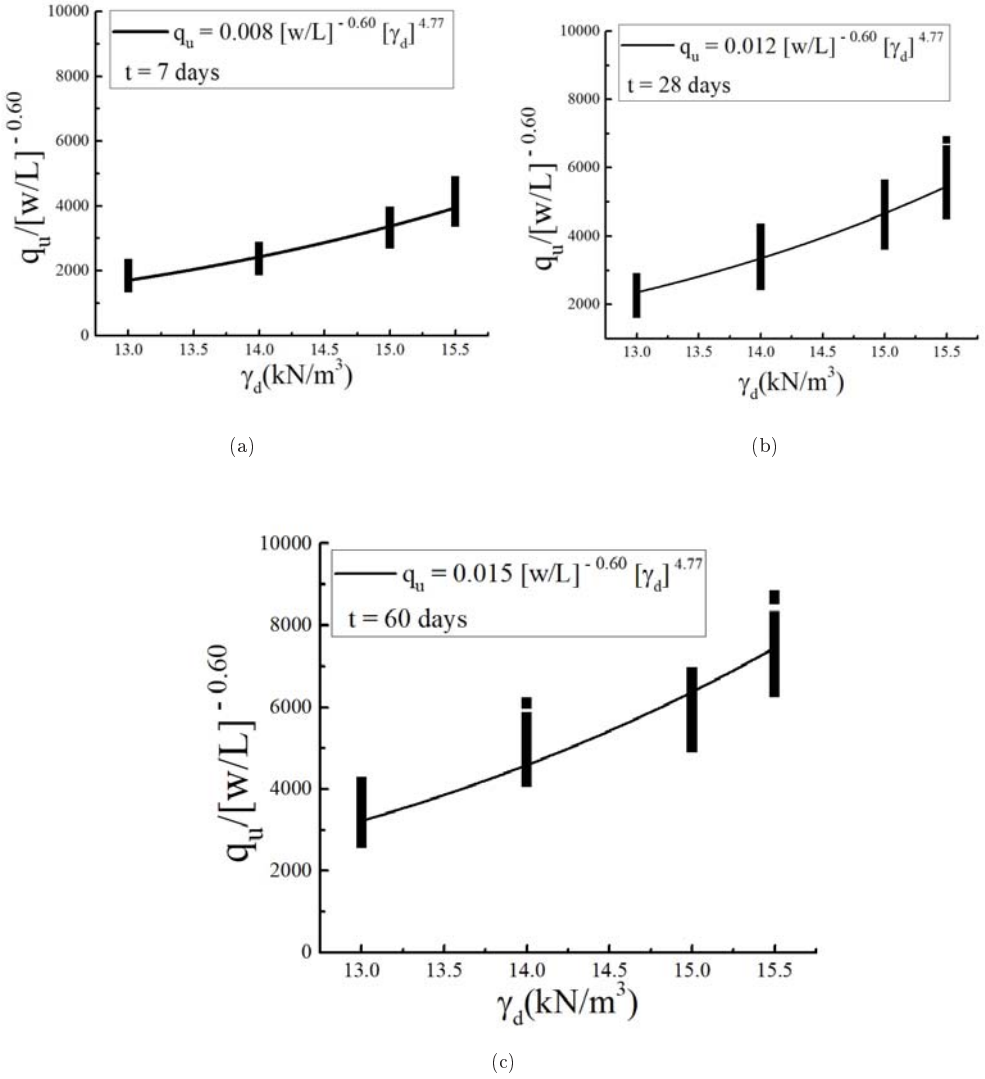

FIGURE 3.9: Variation of $(q_u/(w/L)^{0.60})$ with (γ_d) for curing time (a) 7 days, (b) 28 days and (c) 60 days

The correlation proposed in Eqn.3.18 can be used to achieve the unconfined compressive strength (q_u) of the artificially cemented red mud for the range of studies. However, the cost effective optimal solution may be changed and it shall depend on the site condition, availability of equipment, materials, and workforce. The present findings will give an idea that practicing engineers have many options to reach the target strength (q_u).

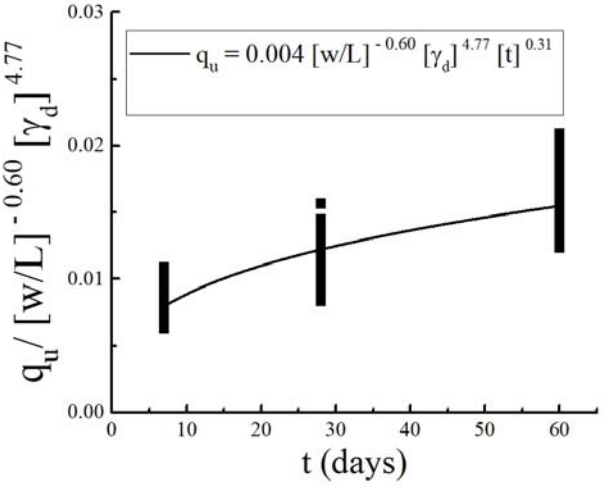

(a)

FIGURE 3.10: unique correlations linking q_u, w, L, γ_d and t

3.4.3.3 Porosity/volumetric lime (η/L_v)

In this section the red mud-lime mix as partially saturated (3 phase soil system) conditions is now considered for study. Thus, porosity/volumetric lime (η/L_v)ratio as fundamental design parameter has been established here to access the unconfined strength of artificially cemented red mud using Eqn.(3.19-3.20) whereas, fundamentals are discussed in details in Eqs. (A.1-A.2)(Appendix B).

$$L_v = 100 \left[\frac{(\frac{\gamma_d}{1+\frac{L}{100}})(\frac{L}{100})}{G_L \gamma_w} \right] \tag{3.19}$$

$$\eta = 100 - 100 \left[\left\{ \frac{\gamma_d}{1+(\frac{L}{100})} \right\} \left\{ \frac{1}{G_R \gamma_w} + \frac{(\frac{L}{100})}{G_L \gamma_w} \right\} \right] \tag{3.20}$$

Where,

η = Porosity (Defined as volume of voids with respect to total volume)

L_v= Volumetric lime content (Defined as volume of lime with respect to volume of specimen)

The influence of porosity and volumetric lime content (porosity/volumetric lime content)(η/L_v) ratio on unconfined compressive strength q_u of red mud-lime mix is shown in Fig. 3.11.

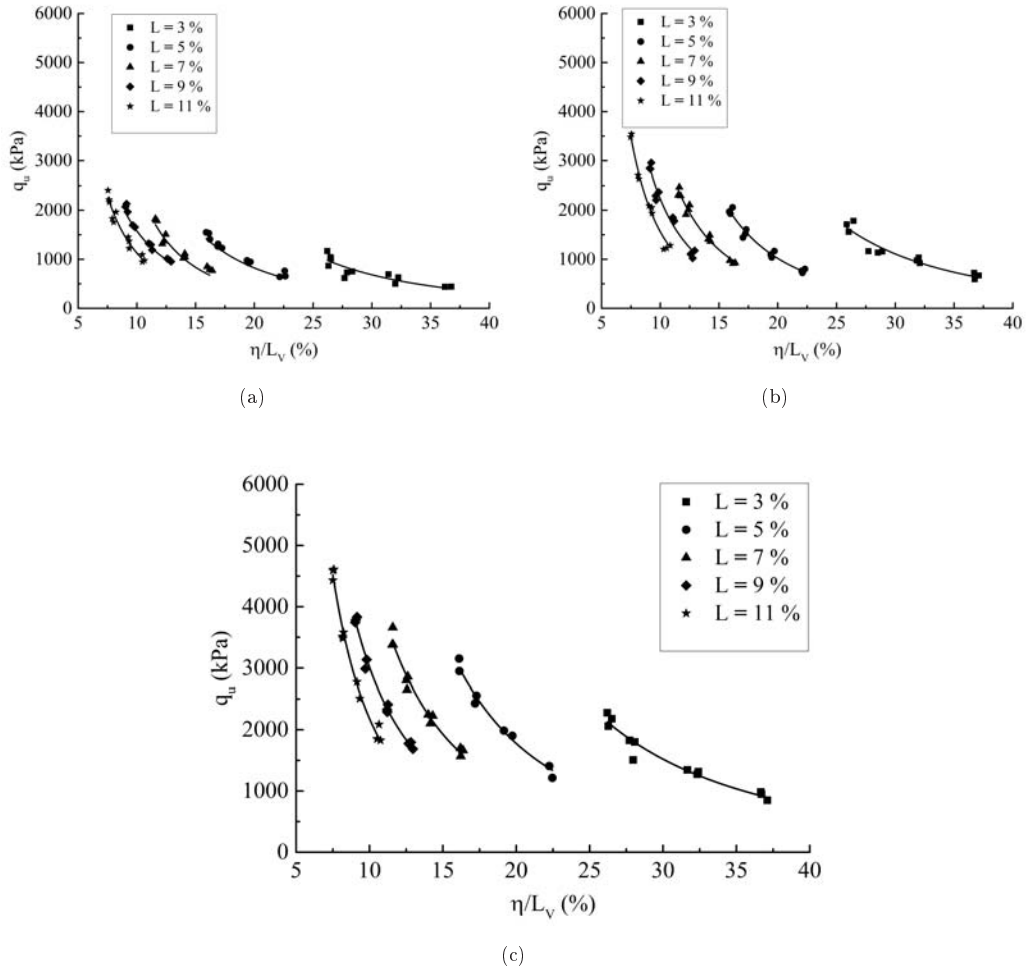

FIGURE 3.11: Effect of porosity/volumetric lime content ratio (η/L_v) on unconfined compressive strength (q_u) of red mud –lime mix with varying curing periods (a) 7 days, (b) 28 days and (c) 60 days

It is seen that for the given red mud-lime mix , there is no meaningful and unique relationship appears between q_u and η/L_v in the present form. It is perhaps

due to different values of q_u is observed by the same porosity/lime ratio but by a different combination of lime and dry density. For example, the value of q_u for η/L_v = 16.13 is 836.96 kPa (for L = 7 % and γ_d = 13.0 kN/m^3), but it changes to 1513.71 kPa with different combination (L = 5 % and γ_d = 15.5 kN/m^d see Fig.3.11(b)). Thus, it is necessary to study η vs.q_u and $1/L_v$ vs. q_u to make the ratio η/L_v with q_u compatible for the range of studies. The individual effect of η and $1/L_v$ with (q_u) for given moisture content (w = 30 %) and various curing time (7, 28 and 60 days) are shown in Figs.3.12 and 3.13 respectively.

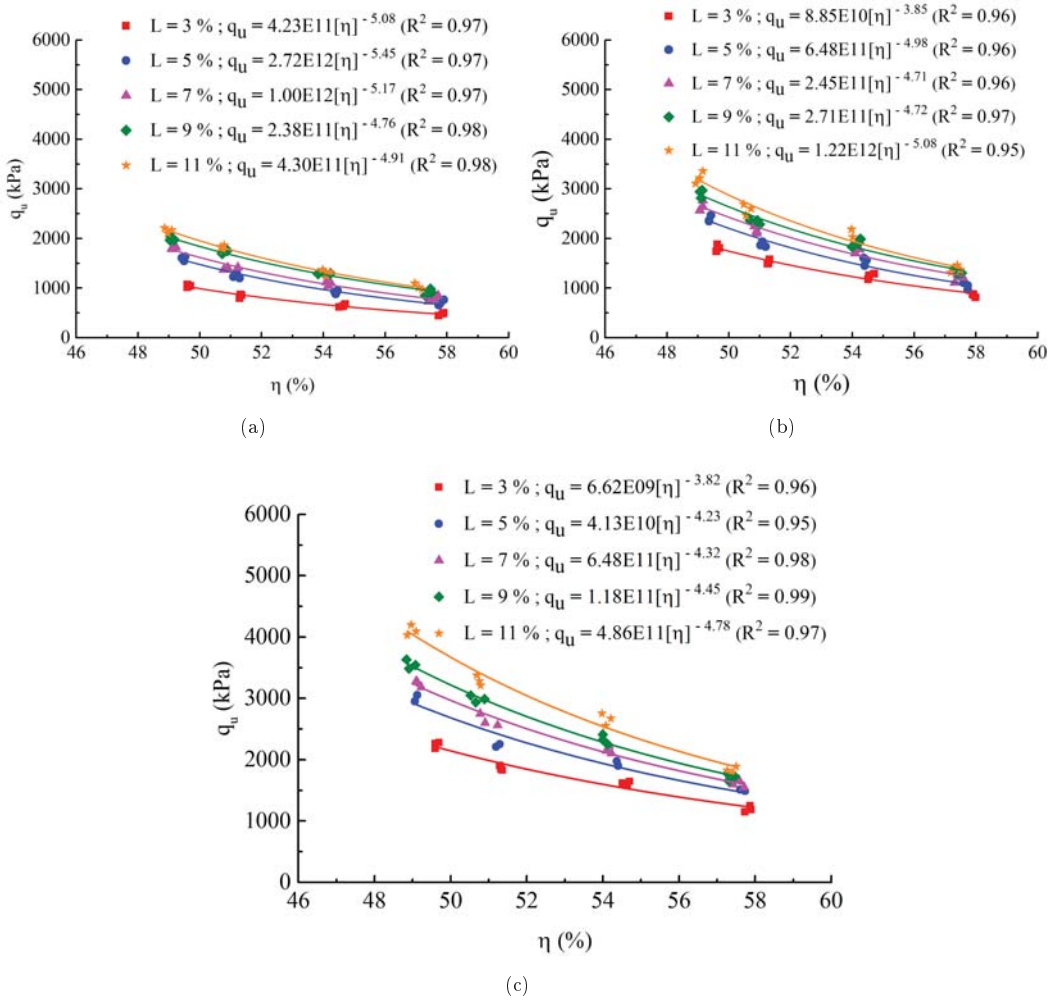

FIGURE 3.12: Variation of η with q_u with varying curing periods (a) 7 days, (b) 28 days and (c) 60 days

From scatter plot shown in Fig.3.12(a), it can be seen that a power model fits well with a good correlation ($R^2 \geq 0.85$) between η with q_u. It also reveals that the value of q_u increases with the decrease in η for the range of studied and a similar trend is observed for other curing periods too. This is attributed to the availability of higher number of contacts leading to the formation of a complex matrix of red mud-lime mixture. Similarly,a plot of q_u and $1/L_v$ is also presented in Fig.3.13) to study the trend of these parameters.

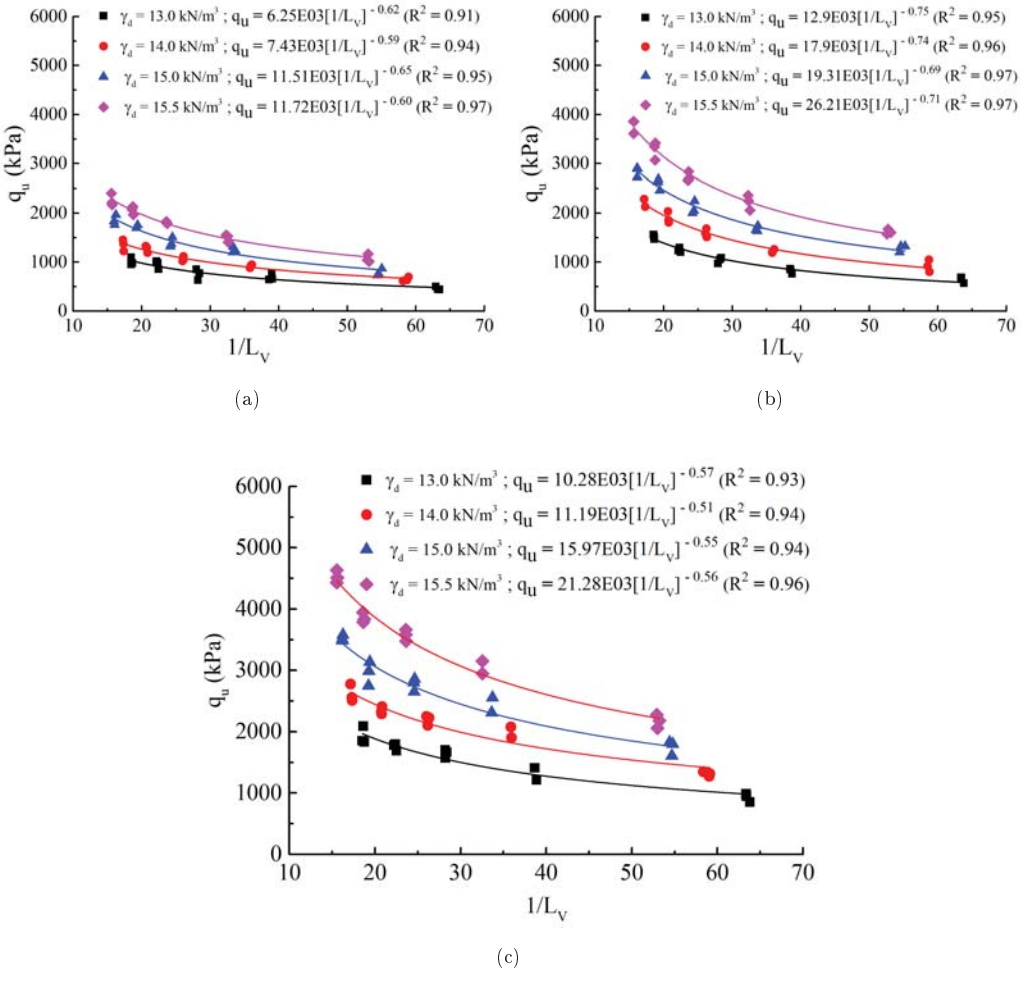

FIGURE 3.13: Variation of inverse of L_v with q_u with varying curing periods (a) 7 days, (b) 28 days and (c) 60 days

Similar trends as above is seen here also in case of q_u with $1/L_v$ (Fig.3.13). The increase in red mud-lime mix strength with the reduction in the inverse of volumetric lime content may be due the availability of higher volume of lime for chemical (pozzolanic) reactions to take place, leading to the formation of cementing gel, which binds the particles of red mud-lime mix. Other researcher reported similar observations as decrease in the unconfined compressive strength with increase in inverse of the lime volume where the effect of inverse volumetric lime content on lime-stabilized soil [234]. From Figs.(3.12-3.13), it can be concluded that the trend of variation of q_u with η and q_u with $1/L_v$ is qualitatively same (i.e. power model) but quantitatively different.

In order to make the variation of η and $1/L_v$ compatible, a power is required to be applied on one of the variables i.e. porosity (η), or volumetric lime (L_v). In present case, an exponent on L_v has been applied to introduce compatibility among the parameters and the value of exponent equal to 0.11 is chosen by trial and observe approach. The procedure followed here are shown in Table 3.2 and presented in Fig. 3.14.

TABLE 3.2: Method for optimize the exponent

Trial	Value of exponent	R^2
1	0.09	0.9625
2	0.095	0.9682
3	0.10	0.9713
4	0.105	0.9720
5	0.11	0.9723
6	0.12	0.9718

Further, the trends are adjusted to close to the average value of all exponent (4.47) to compare the different trends of $\eta/L_v^{0.11}$ with (q_u) and the results are presented in Fig.3.15 and Eqs. (3.21-3.29).

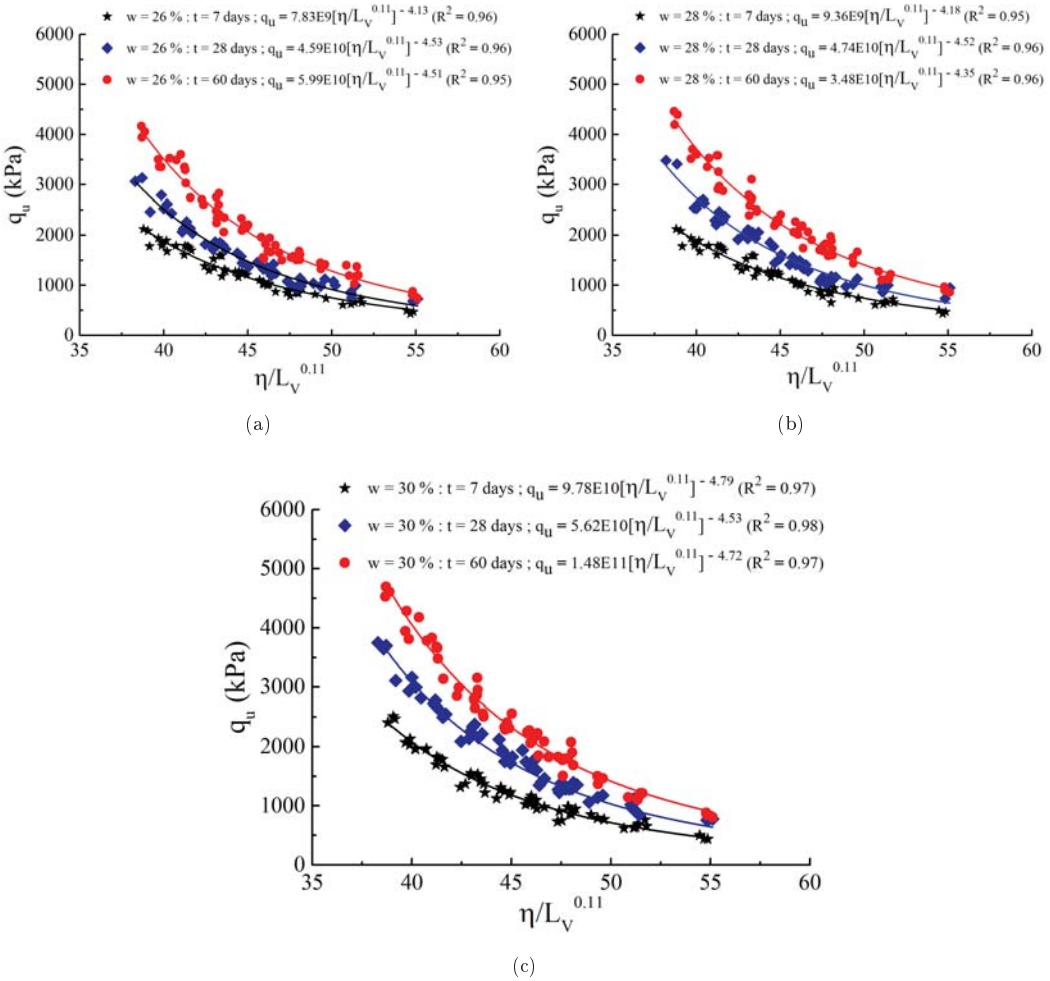

FIGURE 3.14: Variation of adjusted adjusted porosity/volumetric lime content ratio ($\eta/L_v^{0.11}$) on unconfined compressive strength (q_u) with varying moisture content (a) 26 %, (b) 28 % and (c) 30 %

For $w = 26$ %

$$t = 7\,days;\ q_u = 2.78E10\ \left[\eta/L_v^{0.11}\right]^{-4.47} \tag{3.21}$$

$$t = 28\,days;\ q_u = 3.63E10\ \left[\eta/L_v^{0.11}\right]^{-4.47} \tag{3.22}$$

$$t = 60\,days;\ q_u = 5.09E10\ \left[\eta/L_v^{0.11}\right]^{-4.47} \tag{3.23}$$

For $w = 28$ %

$$t = 7\,days;\ q_u = 2.81E10\ \left[\eta/L_v^{0.11}\right]^{-4.47} \tag{3.24}$$

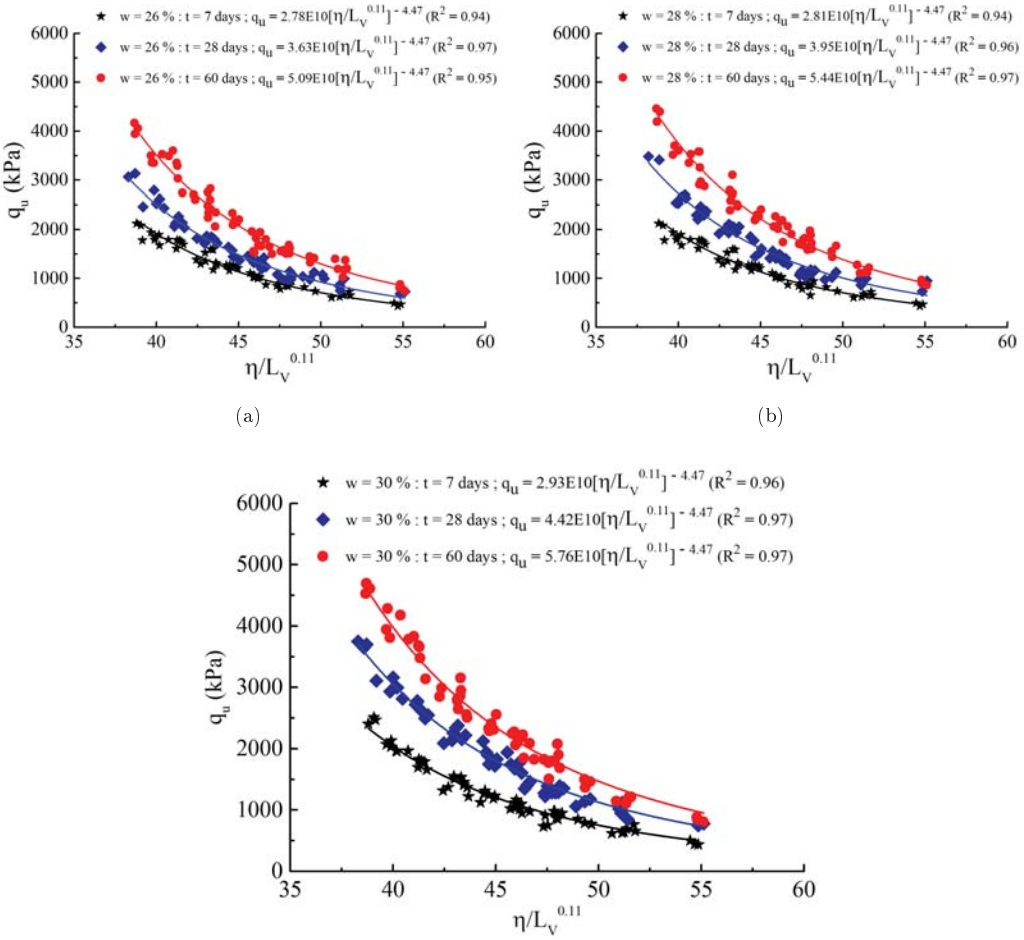

FIGURE 3.15: q_u vs $\left[\eta/L_v^{0.11}\right]^{-4.47}$ plots for different moisture content (a) 26 %, (b) 28 %, and (c) 30 %

$$t = 28\,days;\ q_u = 3.95E10\ \left[\eta/L_v^{0.11}\right]^{-4.47} \tag{3.25}$$

$$t = 60\,days;\ q_u = 5.44E10\ \left[\eta/L_v^{0.11}\right]^{-4.47} \tag{3.26}$$

For $w = 30$ %

$$t = 7\,days;\ q_u = 2.93E10\ \left[\eta/L_v^{0.11}\right]^{-4.47} \tag{3.27}$$

$$t = 28\,days;\ q_u = 4.42E10\ \left[\eta/L_v^{0.11}\right]^{-4.47} \tag{3.28}$$

$$t = 60\,days;\ q_u = 5.76E10\ \left[\eta/L_v^{0.11}\right]^{-4.47} \tag{3.29}$$

Further, it is apparent that q_u has a direct relationship with $[\eta/L_v^{0.11}]^{-4.47}$ and it differs by a scalar for the range of moisture content and curing time studied. The results presented in the Eqs. (3.21-3.29) suggest that by using η/L_v practicing engineer can choose appropriate amount of lime and porosity (for the range of studies) to meet the strength criteria required in any project. The study of above equations further shows that for a given moisture content q_u has direct relationship with $[\eta/L_v^{0.11}]^{-4.47}$ for different curing periods and it differs by a scalar value due to the effect of curing time. For example, for w = 26 % and t = 7 days, the scalar value linking q^u and $[\eta/L_v^{0.11}]^{-4.47}$ was 2.78E10 which increased to 3.63E10 and 5.09E10 with the increase in curing time to 28 and 60 days respectively. Using same procedure as stated above, relationship can also be established among the parameters used in the study. and the details are presented in Fig. 3.16 and Eqs (3.30-3.32).

$$w = 26\,\%;\ q_u = 1.74E10\ \left[\eta/L_v^{0.11}\right]^{-4.47}[t]^{0.29} \tag{3.30}$$

$$w = 28\,\%;\ q_u = 1.87E10\ \left[\eta/L_v^{0.11}\right]^{-4.47}[t]^{0.29} \tag{3.31}$$

$$w = 30\,\%;\ q_u = 1.94E10\ \left[\eta/L_v^{0.11}\right]^{-4.47}[t]^{0.29} \tag{3.32}$$

Finally, a distinctive relationship among the parameters q_u, η, L_v, t and w has been established and proposed and shown in Fig. 3.17 and in Eq.3.33.

$$\boxed{q_u = 1.49E9\ \left[\eta/L_v^{0.11}\right]^{-4.47}[t]^{0.29}[w]^{0.75}} \tag{3.33}$$

As per the established correlations as presented in Eq.3.18 and Eq.3.33, it can be useful and alternative tool to predict the unconfined compressive strengths of red mud-lime mix. Further, it will also offer as dosage methodology for practicing

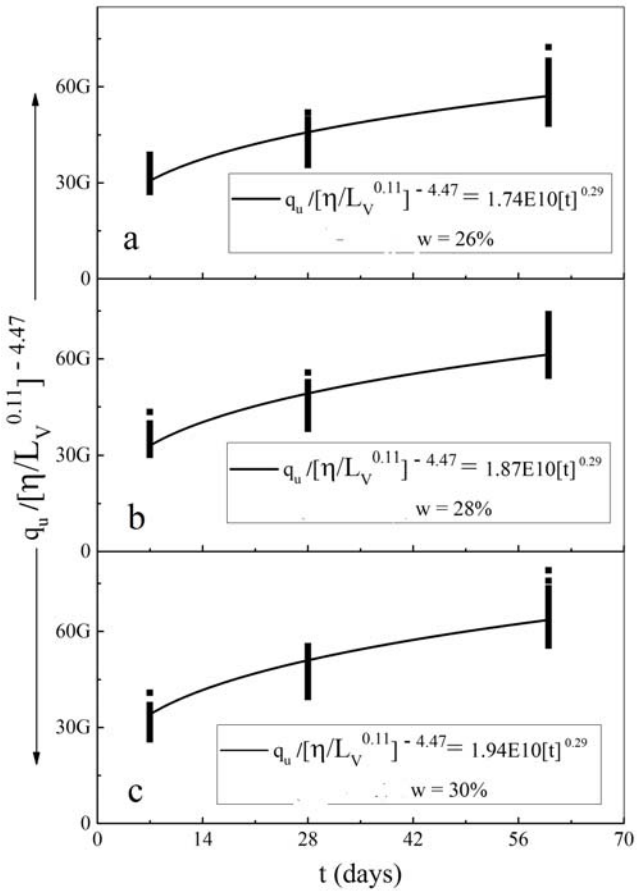

(a)

FIGURE 3.16: $\left[\eta/L_v^{0.11}\right]^{-4.47}$ vs. $[t]^{0.29}$ plots for different curing time and different moisture content

geotechnical engineers for the range of moisture content, lime content, porosity and curing time studied. From above discussion, it can also be said that porosity, amount of lime, molding moisture and curing time are the key parameters that control compressive strengths of red mud-lime mix. However, performing large number of experiments and recording data for multi variables using conventional approach is some time time consuming and expansive. So, to overcome these problem, an attempt has been made to evaluate and compare the strength of stabilized red mud using design of experiment.

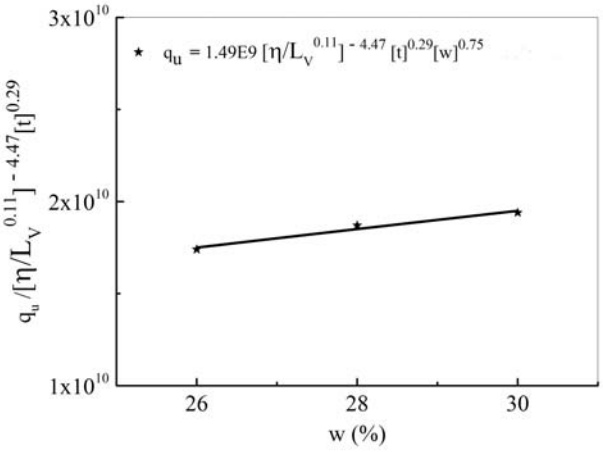

(a)

FIGURE 3.17: Relationship linking q_u, η, L_v, t and w

3.5 Compressive Strength of Stabilized Red Mud: Experimental Designed Approach

3.5.1 Design Methodology

Different experiment design methods may be used for the design of the experiment but it solely depends on the the nature and operability region of the problem. In this study, central composite (CC) and Box-Behnken (BB) design are used to design the experiment. The methodology of design of experiment is discussed in detail in Chapter 2, Sec.2.6.2. The schematic 2-dimensional representations of various central composite and Box-Behnken design are shown in Fig 3.18.

The design of experiment using circumscribed central composite design is not possible in the present case because it needs negative α. For example, a minimum 30 number of experiments is required for four independent variables and some of the experiments need $\alpha = -2$ which is not possible for some of the independent variables

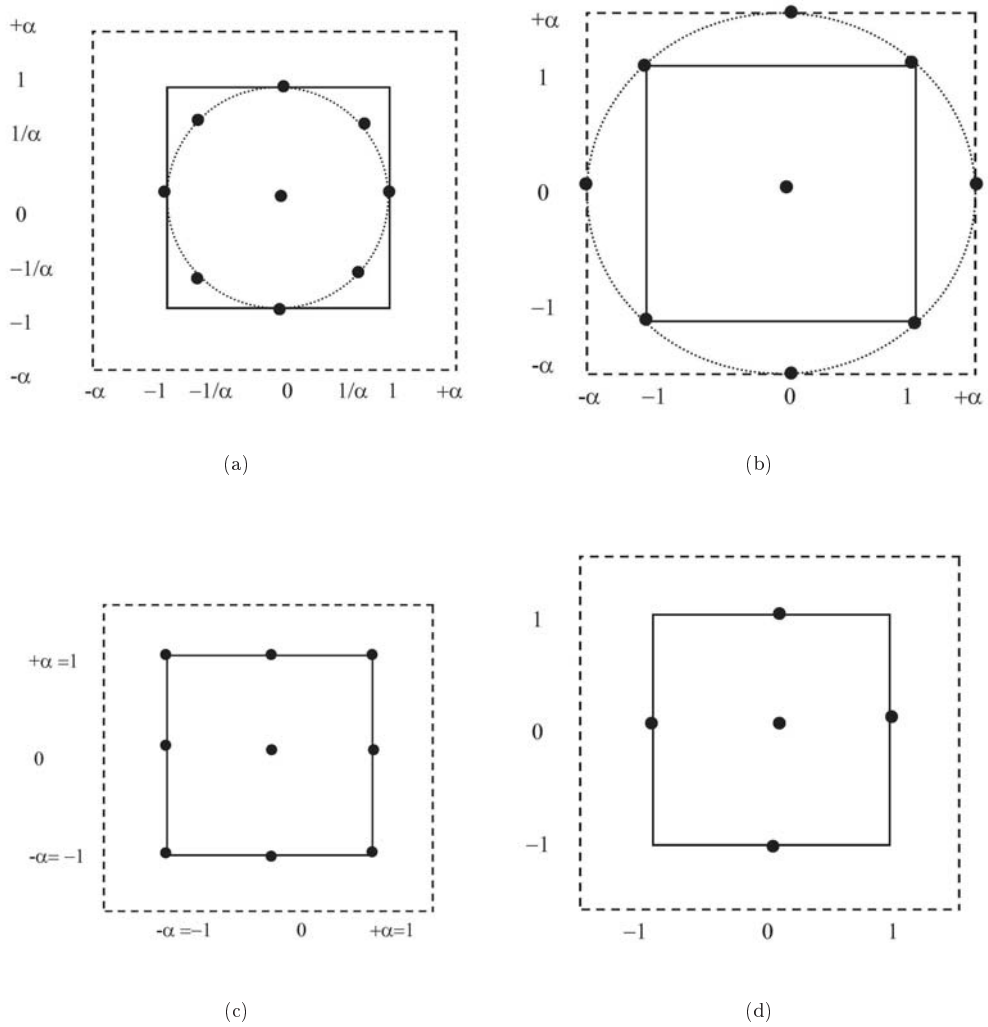

FIGURE 3.18: Schematic diagram of various design of experiment (a) Inscribed central composite (ICC), (b) Circumscribed central composite (CCC), (c) Faced central composite (FCC) and (d)Box-Behnken (BB) design

such as lime content and curing time. Whereas, inscribed central composite design method does not consider some of the extreme points. In view of the limitations, central composite (FCC) and Box-Behnken (BB) designs methods are chosen for the present study. Input variables employed for this study are the lime content (L) and molding moisture (w) in percentage, dry density (γ_d) in kN/m^3 and curing time (t) in day. The operating ranges are taken as 3 to 11% for L, 26 to 30% for w, 13 to

TABLE 3.4: Experimental levels of independent variables for different correlations

Study Type	Input Parameter	Range		
		-1	0	1
A	w	26	28	30
	L	3	7	11
	γ_d	13	14.3	15.5
	t	7	34	60
B	w/L	2.36	6.18	10
	γ_d	13	14.3	15.5
	t	7	34	60
C	$\eta/L_{v'}$	40	48	56
	w	26	28	30
	t	7	34	60

15.5 kN/m^3 for γ_d and 7 to 60 days for t. The experimental levels of independent variables are given in Table 3.4.

The Design-Expert 10 by Stat-Ease Inc., a free statistical software package, is used for the experiment design.

3.5.2 Design matrix and Predictive Equations

After selecting the appropriate design of experiment technique, entire experiments are designed for different variables and are presented in Table 3.5. Based on the experimental design, laboratory tests are performed and results are recorded for each combinations. Results of the laboratory tests are presented as the response in Table 3.5 .

After successful experimental design and development, a predictive equation is required to establish the relationship between input parameters and response for the range of study. Therefore, it becomes important to build a predictive equation that is best suited with experimental results. Thus, various linear and non-linear empirical models were tried and the details are presented in Table 3.6. Further, the

TABLE 3.5: Design matrix of input and response of FCC and BB design methods

Faced central composite (FCC)						Box- Behnken (BB)					
Experimental program						Experimental program					
Run No	Input Parameters				Response	Run No.	Input Parameters				Response
	w	t	γ_d	L	UCS (kPa)		w	t	γ_d	L	UCS (kPa)
1	-1	1	-1	1	1891.48	1	1	0	0	1	2381.09
2	-1	-1	1	-1	947.47	2	0	1	0	-1	1679.35
3	-1	1	-1	-1	988.648	3	1	0	1	0	2295.68
4	0	0	0	0	1776.36	4	0	0	0	0	1576.36
5	0	0	0	0	1864.13	5	0	0	0	0	1464.13
6	1	0	0	0	1487.03	6	0	0	0	0	1531.05
7	1	-1	-1	1	1061.36	7	0	1	0	1	2568.24
8	-1	1	1	-1	1988.98	8	0	0	1	1	3335.25
9	1	-1	1	-1	1117.62	9	1	0	0	-1	1108.35
10	-1	1	1	1	4050.16	10	-1	0	-1	0	947.02
11	1	1	-1	1	1314.87	11	0	-1	1	0	1704.47
12	0	0	0	-1	987.681	12	0	-1	0	-1	702.14
13	-1	0	0	0	1349.41	13	0	0	0	0	1347.08
14	-1	-1	1	1	2047.08	14	1	0	-1	0	1123.16
15	0	1	0	0	2028.6	15	-1	1	0	0	2214.05
16	0	-1	0	0	1492.73	16	0	0	0	0	1482.51
17	-1	-1	-1	1	941.81	17	0	0	0	0	1525.4
18	0	0	1	0	2075.17	18	0	1	1	0	3308.29
19	0	0	0	0	1631.05	19	0	-1	-1	0	838.59
20	-1	-1	-1	-1	480.706	20	0	-1	0	1	1387.41
21	1	-1	-1	-1	502.686	21	1	-1	0	0	1124.23
22	0	0	0	0	1847.08	22	1	1	0	0	2189.8
23	0	0	0	0	1782.51	23	-1	0	0	-1	997.38
24	1	1	1	-1	2171.58	24	-1	-1	0	0	1051.8
25	0	0	0	1	2318.76	25	0	0	-1	-1	737.26
26	0	0	0	0	1825.42	26	-1	0	0	1	1856.25
27	1	-1	1	1	2173.69	27	1	0	1	0	2537.24
28	1	1	-1	-1	925.795	28	0	1	-1	0	1549.35
29	1	1	1	1	4611.45	29	0	0	1	-1	1725.69
30	0	0	-1	0	1193.19	30	0	0	-1	1	1324.05

TABLE 3.6: Summary of various predictive model based on different DOE methods

Face centered composite (FCC)				
Source	p-value	R^2	Adj R^2	Remarks
Linear	< 0.0001	0.8212	0.7926	Significant
2FI	0.0002	0.9424	0.9143	Opted
Quadratic	0.7483	0.9561	0.9151	Insignificant
Cubic	0.0916	0.9897	0.9574	Aliased
Box- Behnken (BB)				
Source	p-value	R^2	Adj R^2	Remarks
Linear	< 0.0001	0.8979156	0.9240533	Significant
2FI	0.0054579	0.9113484	0.9586189	Significant
Quadratic	0.0064267	0.9382578	0.9786678	Opted
Cubic	0.0351175	0.7909774	0.9922652	Aliased

appropriate predictive equation has been selected based on statistical parameters such as p- value, correlation coefficient(R^2) and correlation adjusted coefficient(R^2). From Table 3.6, it is seen that two factor interaction ($2FI$) and quadratic models better satisfy the statistical criteria in case of faced central composite (FCC) and Box-Behnken (BB) design respectively; and hence selected as predictive equations for the range of study. The selection of the statistically significant input variables after choosing the best predictive model is the key step in the experiment design. It tells us if the independent variables and their interaction have significant influence on the dependent variables. In this case, variance analysis ($ANOVA$) could be beneficial in describing the interactions between variables. Thus, $ANOVA$ was performed to establish the parameters found as statistically significant in the predictive model and their relative contributions to the dependent parameter (response) and the results are presented in Tables 3.7 and 3.8 respectively.

From Tables 3.7 and 3.8, it is also observed that the proposed models contain some statistically insignificant terms which have no active role in the prediction of the response. Hence these term are discarded in during the development of predictive equation. From Table 3.7, it is seen that the variables w, t, γ_d, and L, and their interactions $t \times \gamma_d$, $t \times L$ and $\gamma_d \times L$, are the only significant parameters and

TABLE 3.7: *ANOVA* results for FCC design

Source	Sum of Squares (SS)	Degree of Freedom (df)	Mean Square (MS)	F Value	p-value Prob > F	Remarks
Model	20570000	10	2057000	36.42	< 0.0001	significant
w	254500	1	254500	4.51	0.0471	significant
t	4240000	1	4240000	75.09	< 0.0001	significant
γ_d	7443000	1	7443000	131.81	< 0.0001	significant
L	5834000	1	5834000	103.31	< 0.0001	significant
$w \times t$	4687.56	1	4688	0.083	0.7764	insignificant
$w \times \gamma_d$	213100	1	213100	3.77	0.1561	insignificant
$w \times L$	11504.55	1	11505	0.2	0.6568	insignificant
$t \times \gamma_d$	1227000	1	1227000	21.72	0.0002	significant
$t \times L$	356900	1	356900	6.32	0.0211	significant
$\gamma_d \times L$	982600	1	982600	17.4	0.0005	significant
Residual	1073000	19	56468			
Lack of Fit	903200	14	64511	2.99	0.116	not significant
Pure Error	107700	5	21544			
Cor Total	22460000	29				

TABLE 3.8: *ANOVA* results for BB design

Source	Sum of Squares (SS)	Degree of Freedom (df)	Mean Square (MS)	F Value	p-value Prob > F	Remarks
Model	1.36×10^7	14	9.68×10^5	83.09	< 0.0001	significant
w	1.01×10^5	1	1.01×10^5	8.68	0.01	significant
L	2.90×10^6	1	2.90×10^6	249.23	< 0.0001	significant
γ_d	5.86×10^6	1	5.86×10^6	503.3	< 0.0001	significant
t	3.74×10^6	1	3.74×10^6	321.22	< 0.0001	significant
$w \times L$	4.3×10^4	1	4.3×10^4	3.68	0.0744	not significant
$w \times \gamma_d$	1.07×10^3	1	1.07×10^3	0.0919	0.766	not significant
$w \times t$	2.3×10^3	1	2.3×10^3	0.2006	0.6606	not significant
$L \times \gamma_d$	2.62×10^5	1	2.62×10^5	22.45	0.0003	significant
$L \times t$	1.04×10^4	1	1.04×10^4	0.8899	0.3604	not significant
$\gamma_d \times t$	1.99×10^5	1	1.99×10^5	17.12	0.0009	significant
w^2	1.05×10^4	1	1.05×10^4	0.9011	0.3575	not significant
L^2	8.9×10^3	1	8.9×10^3	0.7704	0.3939	not significant
${\gamma_d}^2$	3.92×10^5	1	3.92×10^5	33.66	< 0.0001	significant
t^2	6.9×10^4	1	6.9×10^4	5.96	0.0276	significant
Residual	1.75×10^5	15	11647.39			
Lack of Fit	1.43×10^5	10	14319.33	2.27	0.189	not significant
Pure Error	31517.56	5	6303.51			
Cor Total	1.37×10^7	29				

the main contributing factors in the estimation of unconfined compressive strength. Hence, entire insignificant factors are discarded and only significant parameters are considered for the development of predictive equations. Finally, The basic mathematical equations to predict the response variable (UCS) can be written as Eqs. 3.34 and 3.35:

$$\begin{aligned} q_u = {} & 2071.45 + 12.60w - 109.86t - 140.49\gamma_d - 682.64L + 8.31t \times \gamma_d \\ & + 1.54t \times L + 54.32\gamma_d \times L \end{aligned} \tag{3.34}$$

$$\begin{aligned} q_u = {} & 31558.15 - 44.63w - 967.89L - 4214.54\gamma_d - 83.67t + 12.93w \times L \\ & + 51.14L \times \gamma_d + 6.74\gamma_d \times t + 147.01\gamma_d^2 + 0.13t^2 \end{aligned} \tag{3.35}$$

Other predictive models are also developed using the same procedure as described above and all experimental details are summarized in Tables (B.1-B.8) (Appendix B). Predictive equations linking w/L, t, γ_d and q_u) are presented in Eqs. 3.36 and 3.37. Also, predictive equation linking $\eta/L_v^{0.11}$, t, w and q_u are presented in Eqs. 3.38- 3.39.

$$\begin{aligned} q_u = {} & -7107.84 + 525.42\frac{w}{L} + 606.21\gamma_d - 47.58t - 43.82\frac{w}{L} \times \gamma_d - 1.49\frac{w}{L} \times t \\ & + 5.40\gamma_d \times t \end{aligned} \tag{3.36}$$

$$\begin{aligned} q_u = {} & -6421.71 + 142.73\frac{w}{L} + 582.34\gamma_d - 11.35t - 26.92\frac{w}{L} \times \gamma_d - 0.87\frac{w}{L} \times t \\ & + 2.53\gamma_d \times t + 10.61\left(\frac{w}{L}\right)^2 \end{aligned} \tag{3.37}$$

$$q_u = 10562.89 + 601.87w + 102.98t - 696.63651\frac{\eta}{L_v^{0.11}} - 11.35w \times \frac{\eta}{L_v^{0.11}} - 1.68t \times \frac{\eta}{L_v^{0.11}} + 9.51(\frac{\eta}{L_v^{0.11}})^2 \tag{3.38}$$

$$q_u = 25526.68 + 11.59w + 135.91t - 981.971\frac{\eta}{L_v^{0.11}} - 2.30t \times \frac{\eta}{L_v^{0.11}} + 9.47(\frac{\eta}{L_v^{0.11}})^2 \tag{3.39}$$

3.6 Performance Study

The efficacy of the present models in predicting the unconfined compressive strength of stabilized red mud is checked with the selected data sets. Further, all predictive equations based on conventional and experimental design approach have been designated for easy understanding and detailed in Table 3.9. The scatter plot of measured

TABLE 3.9: Codification of proposed predictive equations

Predictive Equations No.	Designated as	Description
3.2	*CONVA*	Type A predictive equation using based on conventional approach
3.18	*CONVB*	Type B predictive equation based on conventional approach
3.33	*CONVC*	Type C predictive equation based on conventional approach
3.34	*FCCDA*	Type A predictive equation based on face central composite designed approach
3.35	*BBDA*	Type A predictive equation based on Box-Behnken designed approach
3.36	*FCCDB*	Type B predictive equation based on face central composite designed approach
3.37	*BBDB*	Type B predictive equation based on Box-Behnken designed approach
3.38	*FCCDC*	Type C predictive equation based on face central composite designed approach
3.39	*BBDC*	Type B predictive equation based on Box-Behnken designed approach

and predicted UCS is presented in Fig.3.19.

From Fig.3.19, it is seen that the predicted values are close to the measured values. Further, to check the adequacy of the proposed models, different statistical parameters such as maximum absolute error (MAE), average absolute error (AAE),

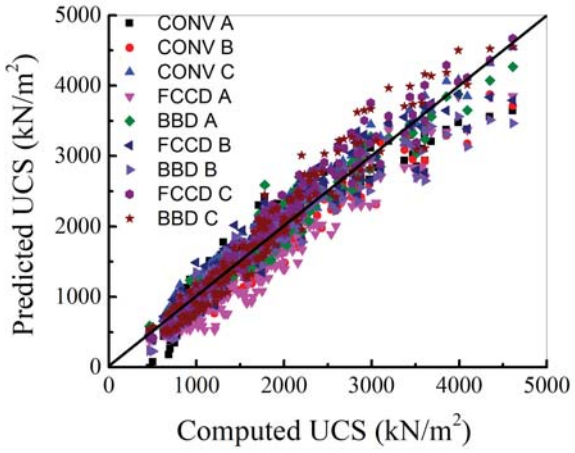

FIGURE 3.19: Scatter plot between computed and predicted values of unconfined compressive strength of stabilized red mud.

root mean square error ($RMSE$), mean absolute percentage error ($MAPE$) and coefficient of determination (R^2) have also been computed to predict the prediction performance of the proposed equations and the results are presented in Table 3.10.

TABLE 3.10: Statistical performance indices of different predictive models

Description	Parameters				
	R^2	MAE	AAE	$RMSE$	$MAPE$
$CONVA$	0.89	967.487	203.7948	264.1839	14.08542
$CONVB$	0.93	916.6567	217.6972	271.1726	12.97904
$CONVC$	0.96	477.5642	149.6609	187.9628	9.866851
$FCCDA$	0.93	910.36	346.1966	391.5644	22.40031
$BBDA$	0.95	810.5025	139.5381	184.0453	8.724423
$FCCDB$	0.92	842.9491	178.5538	240.9237	10.83353
$BBDB$	0.91	1147.151	170.4375	244.7479	10.6359
$FCCDC$	0.96	762.4917	165.1482	214.3276	10.09296
$BBDC$	0.93	810.8371	205.9975	264.5649	12.55937

It can be seen from Table 3.10 that R-squared (R^2) is comparable with all designed approach. Further, other parameter such as $MAPE$ measures the prediction accuracy of the proposed equations. It states that the proposed predictive

model will be excellent, fair or poor fit with the actual data set if the error is less than 10%, 10%-20% and higher than 20% respectively. The values of $MAPE$ of all models except $FCCDA$ are less than 20% confirming that the proposed equations perform satisfactorily. Additionally, scaled percent error (SPE) vs.commulative frequency and Taylor plot have also been incorporated to ascertain the reliability of the predictive equations and presented in Figs. 3.20 and 3.21 respectively. The merits of the above plots as a performance index have been discussed in Sec. 2.9.2 .

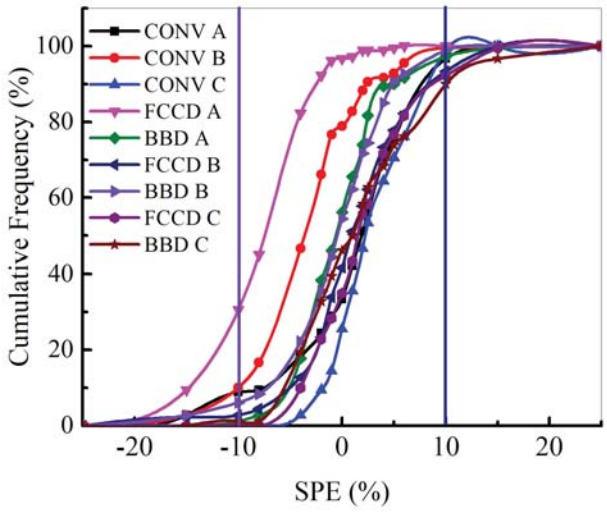

FIGURE 3.20: Scaled percent error (SPE) vs.commulative frequency plot between computed and predicted values of q_u of stabilized red mud.

From Fig. 3.20, it is observed that about 90% of the predicted values of the stability coefficients fall within $\pm 10\%$ of the SPE confirming the reliability of the predictive models. Further, Fig.3.21 also supports the finding obtained in scaled percent error (SPE) vs. commulative frequency plot which concludes that the predictive equation based on experimental designed approach can be used with confidence. Additionally, the main advantage of the application of design of experiment over conventional approach is that the number of experiments in case of DOE is relatively much less than that in conventional designed approach. For example, in the present study, the

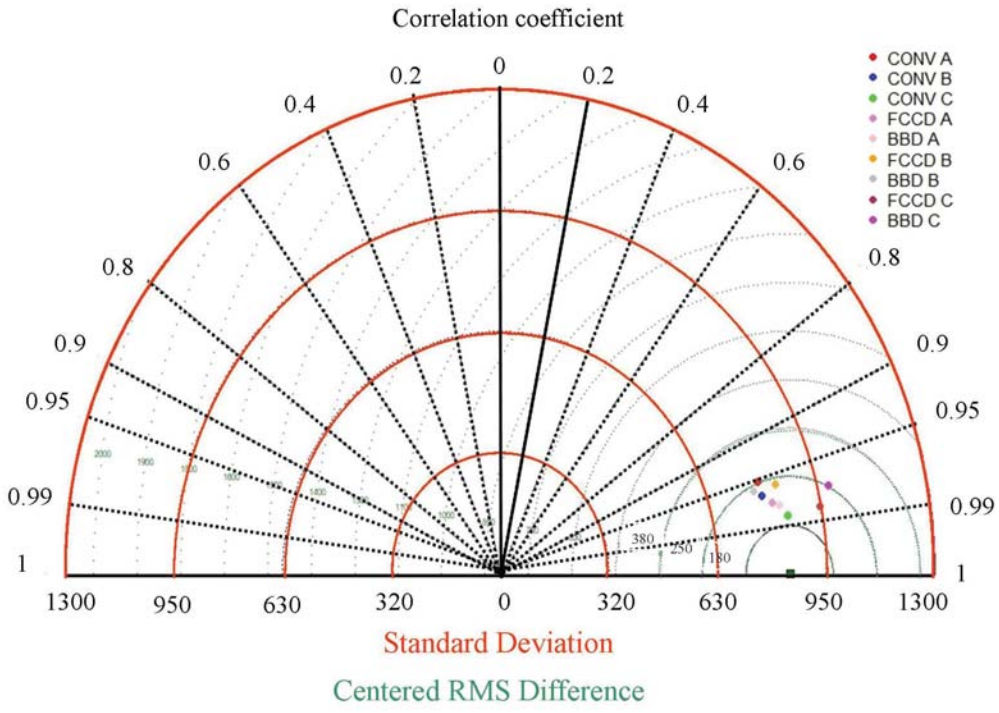

FIGURE 3.21: Taylor plot between computed and predicted q_u of stabilized red mud.

number of experiments used to successfully develop the predictive equations based on conventional designed approach is 180; whereas, in case of experimental designed approaches, it is 30. Therefore, from the above study, it can be concluded that experimental designed approach (DOE) may be considered as an alternative over conventional designed approach for estimating the unconfined compressive strength, it reduces not only the experimentation time but also saves the resources.

3.7 Cross Correlation Study

Cross-correlation study is carried out to find the relative contribution of inputs parameters on response. It also evaluates how the independent parameters influence

the response under given situations. Figure 3.11 shows the relative importance of input parameters on the response based on conventional designed approach. It is

TABLE 3.11: Correlation matrix between the dependent and independent variables

	q_u	w	t	γ_d	L	w/L	$\eta/L_v^{0.11}$
q_u	1.00						
w	0.07	1.00					
t	0.56	0.00	1.00				
γ_d	0.60	0.00	0.00	1.00			
L	0.47	0.00	0.00	0.00	1.00		
w/L	-0.44	0.12	0.00	0.00	-0.92	1.00	
$\eta/L_v^{0.11}$	-0.76	0.00	0.00	-0.78	-0.62	0.61	1.00

observed that lime content, dry density and curing time contributes much more than moisture content on the response (q_u). Further, it is seen that the the parameters such as L, γ_d, t and w influence q_u directly; whereas, parameters like w/L, η/L_v influences indirectly. From Table 3.11, it also infers that the contribution of parameters η/L_v is more as compared to w/L on q_u. However, both parameters η/L_v and w/L can be successfully used to achieve the unconfined compressive strength of the red mud-lime mix but ratio η/L_v can be prefer to reach the target unconfined compressive strength.

From the above studies, it is seen that the experimental designed approach can be successfully applied as an alternative approach to evaluate the unconfined compressive strength of stabilized red mud. So, in the following sections, the study has focused only on experimental designed approach to evaluate the other properties(split tensile strength and durability) of the stabilized red mud.

3.8 Split Tensile Strength Study

Tensile strength of any cemented soil is the key constraint and its durability, brittleness and splitting behavior should be necessarily known before any civil engineering application. The failure mechanism generally starts under tensile stress and failure occurs due to tensile crack in stabilized compacted layer [235]. So, tensile strength can be used to evaluate the mechanical properties of stabilized red mud. In this study, experimental designed approach is also employed to study the split tensile strength of stabilized red mud. The details of results are are given in Tables (B.9-B.11) (Appendix-B). After analysis of data sets, predictive equations have been proposed and are given as Eqs. 3.40-3.41.

$$\begin{aligned} q_t = & -1077.59 + 111.82\frac{w}{L} + 91.70\gamma_d - 15.76t - 9.24\frac{w}{L} \times \gamma_d - 0.37\frac{w}{L} \times t \\ & + 1.504\gamma_d \times t \end{aligned} \tag{3.40}$$

$$q_t = 5056.94 + 6.22w + 17.53t - 198.23\frac{\eta}{L_v^{0.11}} - 0.284t \times \frac{\eta}{L_v^{0.11}} + 1.89(\frac{\eta}{L_v^{0.11}})^2 \tag{3.41}$$

From Eqs. (3.36- 3.39) and Eqs. (3.40-3.41), it is observed that the compressive and tensile strengths have some relation with parameters w/L, η/L_v for the range of studies.

TABLE 3.13: Experimental levels of independent variables for different correlations for wetting and drying study

Study Type	Input Parameter	Range		
		-1	0	1
E	$\frac{w}{L}$	2.36	6.18	10
	γ_d	13	14.3	15.5
	N	2	7	12
	t	7	34	60
F	$\frac{\eta}{L_v{}^{0.11}}$	40	48	56
	w	26	28	30
	N	2	7	12
	t	7	34	60

3.9 Durability Study

Durability of compacted red mud -lime mix was investigated through wetting and drying test to study its endurance . Table 3.13 shows the details of the experimental design based on the faced central composite design methods. Based on the experimental design, laboratory tests are performed and results are recorded for each combinations. The result of the laboratory tests were presented as the response in Table 3.14 for w/L and in Table 3.15 for η/L_v. From wetting-drying results, it is observed that some of the combinations have excessive mass loss after 12 cycles and hence doesn't satisfy the durability criteria (loss of mass less than 30%). Further, looking at the results of wetting-drying of samples (Tables 3.14 and 3.15),it appears that 3% of lime with all dry unit weights, doesn't guarantee endurance of the mix. Thus, 5% lime and dry unit weight of 15.5 kN/m^3 may be the minimum requisite to satisfy the durability requirements.

TABLE 3.14: Design matrix of input and response of FCC design methods using $\frac{w}{L}$ as fundamental parameter for wetting drying studies

Group	Run	$\frac{w}{L}$	N	t	γ_d	Loss of mass (w_L) (%)
1	1	1	1	-1	-1	100
1	2	1	-1	1	1	8.53
1	3	1	1	1	1	16.24
1	4	1	-1	-1	-1	34.61
1	5	1	-1	-1	1	15.84
1	6	1	-1	1	-1	15.08
1	7	1	1	-1	1	39.1
1	8	1	1	1	-1	51.93
2	9	-1	-1	-1	-1	12.38
2	10	-1	-1	1	-1	7.86
2	11	-1	1	-1	1	13.7
2	12	-1	-1	1	1	3.95
2	13	-1	-1	-1	1	4.23
2	14	-1	1	-1	-1	37.55
2	15	-1	1	1	-1	1.09
2	16	-1	1	1	1	7.13
3	17	0	0	0	0	16.83
3	18	0	0	0	0	19.52
3	19	0	0	0	0	16.05
4	20	-1	0	0	0	7.95
4	21	-1	0	0	0	8.39
5	22	1	0	0	0	28.37
5	23	1	0	0	0	26.69
6	24	0	0	0	0	18.09
6	25	0	0	0	0	15.85
6	26	0	0	0	0	17.36
7	27	0	0	0	0	17.02
7	28	0	0	0	0	18.39
7	29	0	0	0	0	17.24
8	30	0	-1	0	0	9.56
8	31	0	0	1	0	14.69
8	32	0	0	0	1	12.3
8	33	0	1	0	0	25.28
8	34	0	0	-1	0	29.05
8	35	0	0	0	-1	31.9

TABLE 3.15: Design matrix of input and response of FCC design methods using $\frac{\eta}{L_v}$ as fundamental parameter for wetting-drying study

Group	Run	$\frac{\eta}{L_v{}^{0.11}}$	N	t	γ_w	Loss of mass (w_L) (%)
1	1	-1	0	0	0	7.71
1	2	-1	0	0	0	6.59
2	3	0	0	-1	0	30.19
2	4	0	0	1	0	15.53
2	5	0	-1	0	0	8.05
2	6	0	1	0	0	27.95
2	7	0	0	0	1	20.91
2	8	0	0	0	-1	17.58
3	9	1	1	-1	-1	80.35
3	10	1	1	-1	1	95.72
3	11	1	-1	1	1	15.39
3	12	1	-1	1	-1	13.51
3	13	1	-1	-1	1	30.19
3	14	1	1	1	1	45.1
3	15	1	1	1	-1	40.91
3	16	1	-1	-1	-1	27.67
4	17	-1	-1	1	1	3.15
4	18	-1	-1	-1	-1	4.83
4	19	-1	1	-1	1	15.98
4	20	-1	1	1	-1	7.85
4	21	-1	-1	-1	1	5.13
4	22	-1	1	-1	-1	13.85
4	23	-1	1	1	1	7.13
4	24	-1	-1	1	-1	3.15
5	25	0	0	0	0	18.59
5	26	0	0	0	0	19.29
5	27	0	0	0	0	18.95
6	28	0	0	0	0	18.19
6	29	0	0	0	0	19.51
6	30	0	0	0	0	17.92
7	31	1	0	0	0	38.02
7	32	1	0	0	0	38.89
8	33	0	0	0	0	18.39
8	34	0	0	0	0	17.52
8	35	0	0	0	0	17.31

3.9.1 Effect of Molding Moisture, Wet-Dry cycle, Curing Time, w/L and η/L_v ratio

From Tables 3.14 and 3.15, it is seen that the loss of mass of the stabilized red mud specimens changes with the change in the Molding Moisture, Curing Time, w/L and η/L_v ratio. Thus, the 3D Response Surface Plots of the variation of the loss of mass of the Mix with different factors are presented in Fig. 3.22 for w/L and in Fig. 3.23 for η/L_v. It is observed that loss of mass increases with the increase in wetting-drying cycles, w/L and η/L_v ratio and decreases with increase in dry density and curing time. Whereas no significant change appears in loss of mass due to change in molding moisture content (w).

In view of the above findings, predictive equations can be established to predict the loss of mass of the stabilized red mud for the range of the studies. The basic mathematical equations to predict the loss of mass are given in Eqs. 3.42 and 3.43 for parameter w/L and η/L_v respectively.

$$\begin{aligned}\sqrt{w_L} = 7.048 + 1.428\frac{w}{L} + 0.505N - 0.173t - 0.336\gamma_d + 0.059\frac{w}{L} \times N - 0.0007\frac{w}{L} \times t \\ - 0.088\frac{w}{L} \times \gamma_d - 0.0034N \times t - 0.0258\gamma_d \times N + 0.0117t \times \gamma_d\end{aligned} \tag{3.42}$$

$$\begin{aligned}\sqrt{w_L} = & -7.554 + 0.061w + 0.064t + 0.189\frac{\eta}{L_v^{0.11}} - 0.329N - 0.0017t \times \frac{\eta}{L_v^{0.11}} \\ & + 0.013N \times \frac{\eta}{L_v^{0.11}} - 0.0018N \times t\end{aligned} \tag{3.43}$$

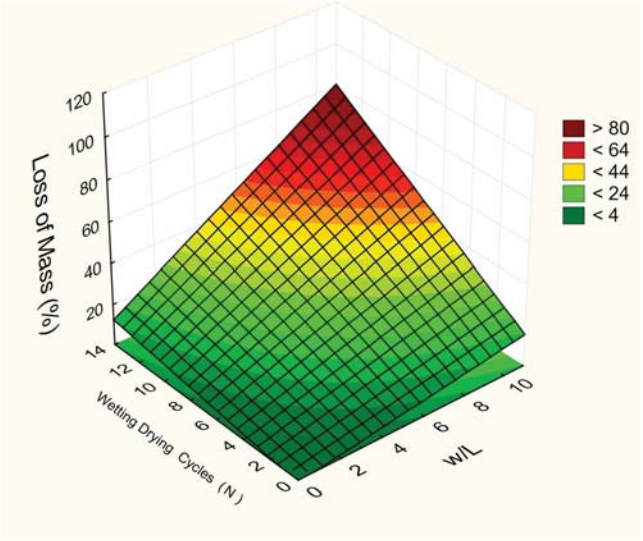

(a)

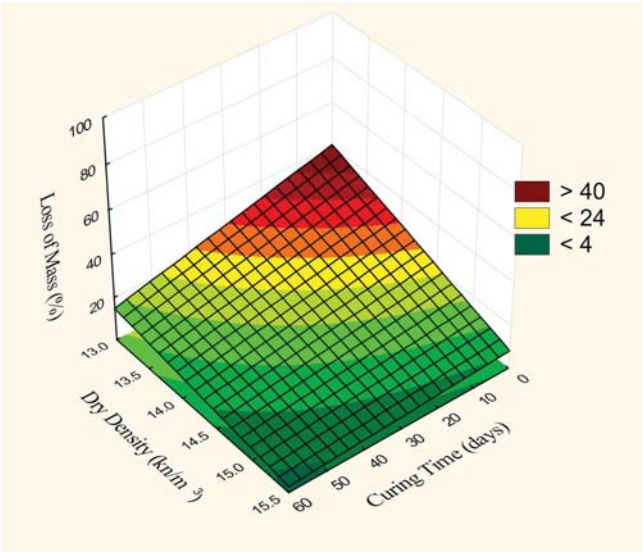

(b)

FIGURE 3.22: The 3D Response Surface Plots of the variation of the loss of mass of the Mix with (a)w/L and N and (b) γ_d and t

3.9.2 Performance Study

The efficacy of the proposed predictive equations is checked with the selected data sets. The scatter plot of measured and predicted loss of mass are presented in

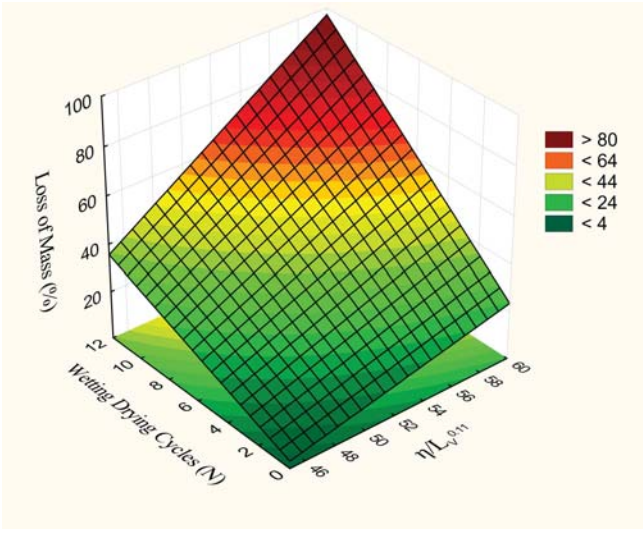

(a)

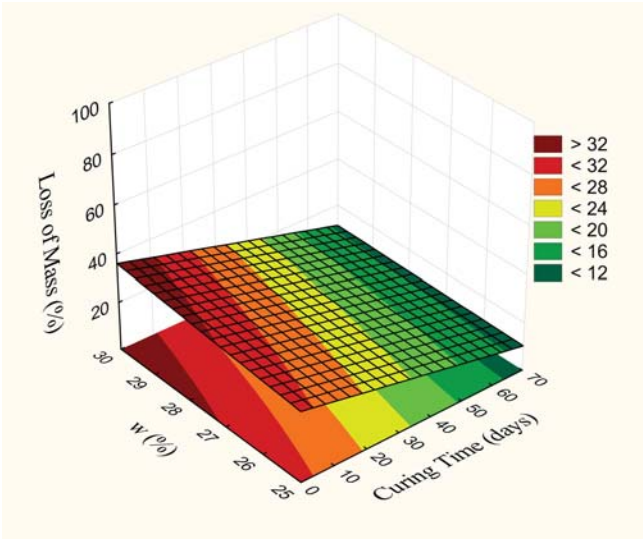

(b)

FIGURE 3.23: The 3D Response Surface Plots of the variation of the loss of mass of the Mix with (a) $\eta/L_v^{0.11}$ and N and (b) t and w

Fig.3.24.

It is observed that all the data points lie very close to the line indicating that the predicted values are very close to the actual value of the selected data sets. Furthermore, scaled percent error (SPE) vs. commulative frequency plot has also

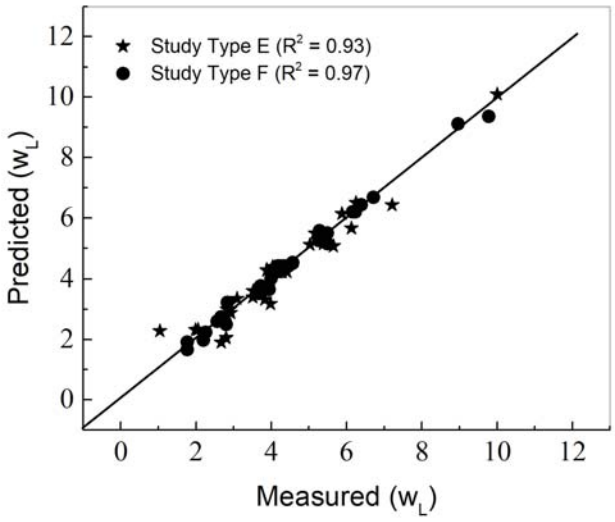

FIGURE 3.24: Scatter plot between computed and predicted loss of mass

been considered to confirm the reliability of the predictive equations and presented in Fig.3.25. It is observed for Fig.3.25 that nearly 95% of the predicted values of

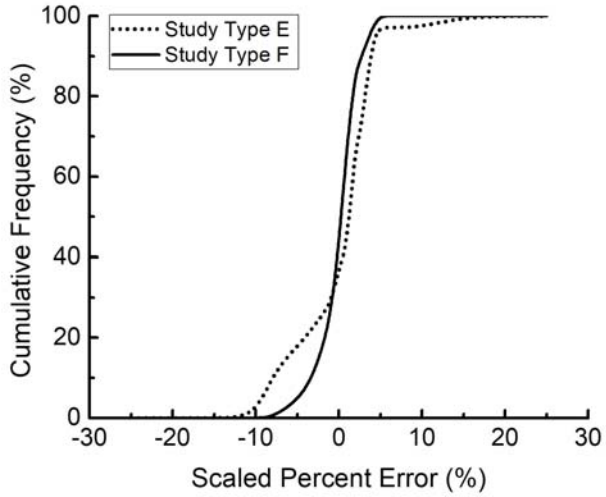

FIGURE 3.25: Scaled percent error vs cumulative frequency plot between computed and predicted values of loss of mass

the loss in mass fall within ±10% of the SPE, thus, confirming the reliability of the predictive equations. Hence, the loss of mass of stabilized red mud using these predictive equations can be used as ready reference for the range of studies.

3.9.3 Optimization Study

The optimization study is required to establish the optimum amounts of the independent variables for the optimal performance (Min, Max or Target) of the stabilized red mud mix for specific applications. The optimum values for the independent and dependent variables were obtained using statistical software package "Design-Expert 10". It has some inbuilt preferences such as "maximum", "minimum", "target" and "in range" for the independent and dependent variables. The optimization study for the independent and dependent variables employed here was performed on the basis of report available in the literature. **Mathur, et al. (2012)** [236] recommended that the soil-cement losses for 12 cycles of wet-dry tests for the use of stabilized material in the base-course, sub-base course or sub-grade are 20% and 30% respectively. Thus, on the basis of the above recommendation, an optimization study was performed for the prediction of the optimum amount of $\frac{w}{L}$, $\frac{\eta}{L_v}$, curing time and wetting-drying cycles in order to obtain the targeted mass loss of the mix. The range for optimization of variables $\frac{w}{L}$, γ_d, w, $\frac{\eta}{L_v^{0.11}}$, t are chosen as 2.36-10, 13-15.5 kN/m^3, 26-30%, 40-56, 7-60 days respectively. Whereas, the maximum number of cycles of wetting-drying cycles are fixed at 12 and the values of mass loss is fixed in accordance with the ranges used by other researchers. Few solutions of optimum values that satisfied the ranges of variables for pavement layers were obtained and presented in Table 3.16.

From the Table 3.16, it is seen that some of the combinations of the mix satisfies the durability criteria and can be recommended for civil engineering applications. However, detailed studies such as field trails are also required to check the endurance of the mix.

TABLE 3.16: Optimized results for application in pavement layers based on study type E and F

Sr. No.	Suitability	Study Type									
		E					F				
		$\frac{w}{L}$	N	t	γ_d	w_L	$\frac{\eta}{L_g^{0.11}}$	N	t	w	w_L
1	Sub-grade/Sub-base Course and Base Course	3.5	12	51	14.9	4.7	40.0	12	60	26.0	6.2
2		3.2	12	59	13.9	6.1	40.0	12	60	30.0	7.5
3		4.5	12	46	15.3	8.0	40.8	12	46	27.2	9.6
4		2.4	12	34	14.3	8.3	42.8	12	59	28.6	11.4
5		2.4	12	60	13.0	8.4	41.7	12	45	29.6	12.5
6		2.5	12	29	14.4	10.1	40.4	12	19	27.3	13.6
7		2.4	12	7	15.5	13.0	40.0	12	7	26.0	14.2
8		3.6	12	28	14.5	14.8	40.0	12	7	30.0	16.1
9		6.2	12	34	15.5	15.9	42.5	12	30	29.9	17.6
10		10.0	12	60	15.5	18.4	42.8	12	28	28.7	18.0
11		6.5	12	57	14.1	19.5	42.2	12	19	28.9	19.0
12		7.5	12	59	14.4	20.0	42.9	12	17	26.1	19.9
13	Sub-grade/Sub-base Course	8.9	12	50	15.1	21.2	48.0	12	60	28.0	21.0
14		6.8	12	29	15.2	22.5	43.2	12	8	26.2	23.1
15		6.2	12	32	14.6	23.7	49.9	12	59	29.7	26.8
16		4.6	12	26	14.1	24.9	48.5	12	48	29.8	28.0
17		7.2	12	20	15.4	25.7	46.8	12	28	26.2	28.2
18		6.2	12	34	14.3	26.7	50.7	12	58	28.8	28.8
19		8.6	12	34	15.0	28.0	44.5	12	10	30.0	29.2
20		7.4	12	52	13.7	29.9	48.0	12	34	26.0	29.7

3.10 Leachate Study

Study of leaching of metals is an important factor for industrial wastes to ensure that the end product is safe or not for the environment. Few selected failed cylindrical UCS specimen of red mud with and without treatment are carried out using atomic absorption spectrophotometer (AAS) and the results are presented in Table 3.17. A close examination of Table 3.17 reveals that the leaching of trace elements are within permissible limit. Thus, these composite mix of red mud can be used as constructional material and may not have any adverse impact on the environment so far these metals are concerned. However, before using these material at actual site , it is suggested to carry out pilot scale studies and field trials for their long term durability and the performance of the mix.

TABLE 3.17: Results of leachate test of red mud with and without treatment

Mix			Trace elements (ppm)					
L(%)	$\gamma_d(kN/m^3)$	t($days$)	Hg	Cd	Cr	Cu	Ni	Pb
Red mud			ND	ND	0.691	0.523	0.496	0.384
7	14.25	7	ND	ND	0.496	0.319	0.321	0.299
11	15.5	7	ND	ND	0.48	0.309	0.318	0.298
11	13	7	ND	ND	0.491	0.335	0.324	0.302
3	13	7	ND	ND	0.533	0.36	0.325	0.313
3	15.5	7	ND	ND	0.581	0.355	0.311	0.299
7	14	28	ND	ND	0.234	0.061	0.038	0.034
11	14	28	ND	ND	0.211	0.043	0.029	0.036
7	13	28	ND	ND	0.279	0.091	0.069	0.061
7	15.5	28	ND	ND	0.195	0.074	0.04	0.054
3	14	28	ND	ND	0.241	0.0841	0.042	0.059
3	15.5	60	ND	ND	0.195	0.069	ND	0.019
7	14	60	ND	ND	0.119	0.039	0.032	0.014
11	13	60	ND	ND	0.128	0.049	0.027	0.019
11	15.5	60	ND	ND	0.095	0.035	0.018	0.025
3	13	60	ND	ND	0.215	0.075	0.031	0.048
Permisible limit, USEPA (ppm)			5	1	2	3	3	5
Note: ND = Not Detected								

3.11 Summary

In the present chapter, different designed approach (conventional and design of experiment) are demonstrated and compared in evaluation of compressive strength of stabilized red mud. Further, different predictive equations using conventional and experimental designed approach are also proposed to reach the strength of stabilized red mud. The efficacy of all the predictive equations are checked using various statistical methods . The different statistical indices shows that all equations are working good for the range of the study which confirm that experimental designed approach can be used with as alternate methods for multivariate study.